Immune cell complexity in the tumor microenvironment of breast cancer
Salvagno, C.

Citation
Salvagno, C. (2019, October 22). *Immune cell complexity in the tumor microenvironment of breast cancer*. Retrieved from https://hdl.handle.net/1887/79824

Cover Page

Universiteit Leiden

Author: Salvagno, C.
Title: Immune cell complexity in the tumor microenvironment of breast cancer
Issue Date: 2019-10-22

CHAPTER 5

Therapeutic targeting of macrophages enhances chemotherapy efficacy by unleashing type I interferon response

Camilla Salvagno[1], Metamia Ciampricotti[1,9,12], Sander Tuit[2,10,12], Cheei-Sing Hau[1], Antoinette van Weverwijk[1], Seth B. Coffelt [1,11], Kelly Kersten[1], Kim Vrijland[1], Kevin Kos[1], Thomas Ulas[2], Ji-Ying Song[3], Chia-Huey Ooi[4], Dominik Rüttinger[5], Philippe A. Cassier[6], Jos Jonkers[7], Joachim L. Schultze[2,8], Carola H. Ries[5] and Karin E. de Visser[1*]

[1]   Division of Tumor Biology & Immunology, Oncode Institute, Netherlands Cancer Institute, Amsterdam, The Netherlands.
[2]   Genomics and Immunoregulation, LIMES-Institute, University of Bonn, Bonn, Germany.
[3]   Division of Experimental Animal Pathology, Netherlands Cancer Institute, Amsterdam, The Netherlands.
[4]   Roche Innovation Center Basel, Roche Pharma Research and Early Development, Basel, Switzerland.
[5]   Roche Innovation Center Munich, Roche Pharma Research and Early Development, Penzberg, Germany.
[6]   Department of Medicine, Centre Léon Bérard, Lyon, France.
[7]   Division of Molecular Pathology, Oncode Institute, Netherlands Cancer Institute, Amsterdam, The Netherlands.
[8]   Platform for Single Cell Genomics and Epigenomics (PRECISE) at the German Center for Neurodegenerative Diseases and the University of Bonn, Bonn, Germany.
[9]   Present address: Molecular Pharmacology Program and Department of Medicine, Memorial Sloan Kettering Cancer Center, New York, NY, USA.
[10] Present address: Department of Anatomy and Embryology, Leiden University Medical Center, Leiden, The Netherlands.
[11] Present address: Cancer Research UK Beatson Institute and Institute of Cancer Sciences, University of Glasgow, Glasgow, UK.
[12] These authors contributed equally: Metamia Ciampricotti, Sander Tuit.
*   e-mail: k.d.visser@nki.nl

Abstract

Recent studies have revealed a role for macrophages and neutrophils in limiting chemotherapy efficacy; however, the mechanisms underlying the therapeutic benefit of myeloid-targeting agents in combination with chemotherapy are incompletely understood. Here, we show that targeting tumour-associated macrophages by colony-stimulating factor-1 receptor (CSF-1R) blockade in the *K14cre;Cdh1^{F/F};Trp53^{F/F}* transgenic mouse model for breast cancer stimulates intratumoural type I interferon (IFN) signalling, which enhances the anticancer efficacy of platinum-based chemotherapeutics. Notably, anti-CSF-1R treatment also increased intratumoural expression of type I IFN-stimulated genes in patients with cancer, confirming that CSF-1R blockade is a powerful strategy to trigger an intratumoural type I IFN response. By inducing an inflamed, type I IFN-enriched tumour microenvironment and by further targeting immunosuppressive neutrophils during cisplatin therapy, antitumour immunity was activated in this poorly immunogenic breast cancer mouse model. These data illustrate the importance of breaching multiple layers of immunosuppression during cytotoxic therapy to successfully engage antitumour immunity in breast cancer.

Main

Poor chemotherapy response is a major obstacle to successful cancer treatment. There is a growing appreciation for the influential role of the immune system on the success of cytotoxic anticancer therapy[1]. Although the adaptive immune system contributes to the therapeutic benefit of certain chemotherapeutic drugs in immunogenic tumour models[2], it frequently fails to be unleashed by these same agents in less immunogenic transgenic mouse tumour models[3,4,5], suggesting the involvement of immunosuppressive mechanisms. Indeed, macrophages and neutrophils are frequently the most abundant immune cells in tumours, and clinical studies have reported a correlation between these myeloid cells and poor chemotherapy efficacy[4,6,7,8,9,10]. Experimental animal studies confirm a causal relationship between tumour-associated myeloid cells and poor chemotherapy response[4,5,11,12,13,14,15,16,17,18,19,20]. For example, inhibition of macrophages in mammary tumour-bearing MMTV-PyMT mice increases paclitaxel efficacy via activation of antitumour immunity[4,5]. Notably, macrophage-targeting and neutrophil-targeting agents are currently under clinical evaluation[21,22,23]. Although promising, the aforementioned preclinical studies only show a transient therapeutic effect of combined myeloid cell targeting and chemotherapy. A deeper understanding of the mechanisms of action is needed to facilitate the rational design of therapeutic combination strategies that convert 'cold' non-T cell-inflamed tumours into 'hot' inflamed tumours, thus engaging durable antitumour immunity in otherwise poorly immunogenic tumours.

By combining in vivo intervention experiments and mechanistic studies in the *K14cre;Cdh1*[F/F]*;Trp53*[F/F] (KEP) mouse model for spontaneous mammary tumorigenesis[24] with validation studies in tumour biopsies of patients treated with anti-colony-stimulating factor-1 receptor (anti-CSF-1R), here, we demonstrate that CSF-1R inhibition synergizes with platinum-based chemotherapy by unleashing an intratumoural type I interferon (IFN) response. Besides this anti-CSF-1R-mediated conversion of the tumour microenvironment (TME) into a type I IFN-enriched milieu, it takes breaching of an additional layer of immunosuppression to engage antitumour immunity during cytotoxic therapy.

Results

CSF-1R blockade does not affect mammary tumour growth or metastasis in KEP mice

We set out to assess the role of CSF-1–CSF-1R signalling, which is vital for macrophages[25], in tumour progression in the KEP model, which spontaneously develops mammary tumours resembling human invasive lobular carcinomas (ILCs) at 6–8 months of age[24]. Similar to human ILCs, KEP tumours are strongly infiltrated by macrophages (Supplementary Fig. 1a,b). Whereas in the MMTV-PyMT breast cancer model it has been reported that two distinct macrophage populations reside within the TME: CD11b^{hi}MHCII^{hi}CD206^{hi} mammary tissue macrophages and CD11b^{lo}MHCII^{hi}CD206^{lo} tumour-associated macrophages (TAMs)[26], in mammary tumours of KEP mice, all F4/80^{+} macrophages express high levels of CD11b, low levels

of CD206 and only a proportion of these cells expresses major histocompatibility complex class II (MHCII) (Supplementary Fig. 1c). These differences in intratumoural macrophage phenotypes between mouse tumour models underscore the complexity of macrophage plasticity in different tumour contexts. In line with the macrophage influx, CSF-1 protein levels are increased in KEP tumours versus healthy mammary glands of age-matched wild-type littermates (Fig. 1a). Both cancer cells and host cells in KEP tumours express *Csf1* mRNA, whereas *Csf1* mRNA is barely detectable in healthy mammary glands (Fig. 1b). CSF-1R is highly expressed on TAMs and to a lesser extent on infiltrating monocytes and neutrophils (Supplementary Fig. 1d), but not on other tumour-associated immune cells or CD45⁻ cells (Supplementary Fig. 1d).

To determine whether intratumoural macrophage accumulation depends on CSF-1–CSF-1R signalling and whether macrophages influence tumour outgrowth and dissemination, we treated tumour-bearing KEP mice with a chimeric mouse IgG1 antagonistic antibody (2G2) that binds to mouse CSF-1R with high affinity (dissociation constant (K_d) = 0.2 nM) or with a control antibody[21]. CSF-1R blockade strongly reduced the TAM population (Fig. 1c,d) and, as a result, also the total CD45⁺ population (Supplementary Fig. 1e). Treatment with anti-CSF-1R alone did not influence tumour-specific survival (Fig. 1f) or spontaneous metastasis formation (Supplementary Fig. 1f). We also investigated the therapeutic activity of anti-CSF-1R in the KEP-based model of spontaneous breast cancer metastasis[27]. In this model, after orthotopic transplantation of a KEP-derived tumour piece followed by surgical removal of the outgrown tumour, mice develop overt multi-organ metastatic disease. Anti-CSF-1R was started either after a palpable mammary tumour had developed (continuous setting) or after mastectomy (adjuvant setting) and continued until the development of metastatic disease (Supplementary Fig. 1g). Regardless of the treatment schedule, metastasis-specific survival and metastatic burden in the lungs were similar between control and anti-CSF-1R groups (Supplementary Fig. 1h,i). Thus, anti-CSF-1R monotherapy fails to affect outgrowth and dissemination of KEP mammary tumours.
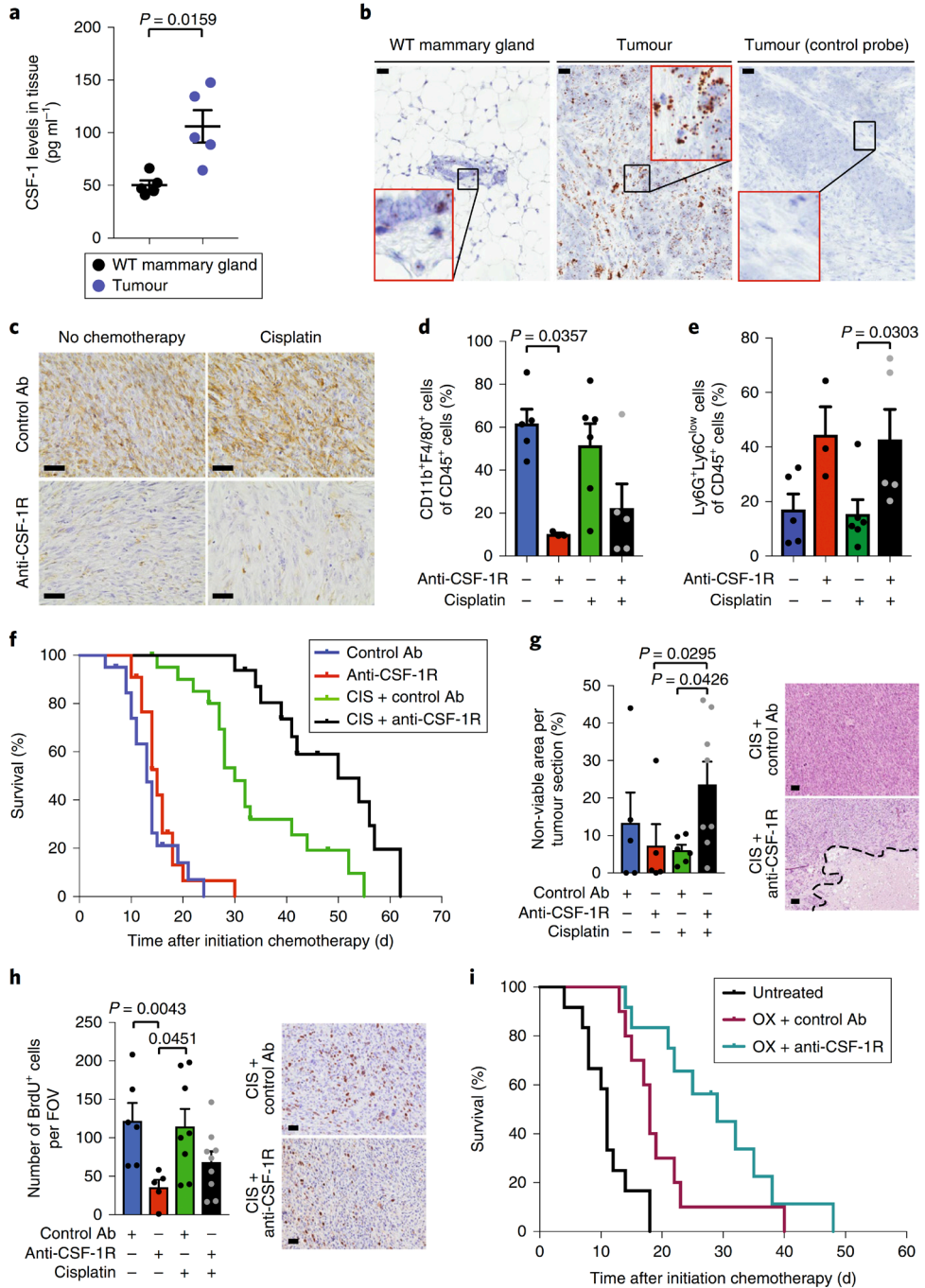
Fig. 1 | CSF-1R blockade improves the anticancer efficacy of platinum-based chemotherapeutic drugs in the KEP mouse model for de novo mammary tumorigenesis.
a, CSF-1 protein levels in end-stage mammary tumours of KEP mice and mammary glands of age-matched wild-type (WT) mice ($n = 5$ animals per group) measured by Luminex cytokine array. **b**,

Representative images of RNA in situ hybridization of *Csf1* (brown signal) in end-stage KEP tumours and normal mammary glands of age-matched WT mice. Data are representative of three animals per group. Scale bars, 25 μm. **c**, Representative immunohistochemistry images of F4/80$^+$ macrophages in tumours of time-point-sacrificed KEP mice treated as indicated. Data are representative of five animals per group. Scale bars, 25 μm. **d,e**, Proportion of CD11b$^+$F4/80$^+$ macrophages (**d**) and Ly6G$^+$Ly6C^{low} neutrophils (**e**) gated on CD45$^+$ cells, as determined by flow cytometry in tumours of end-stage KEP mice treated as indicated (untreated: $n = 5$ animals; anti-CSF-1R: $n = 3$ animals; cisplatin: $n = 6$ animals; cisplatin + anti-CSF-1R: $n = 5$ animals). **f**, Kaplan–Meier tumour-specific survival curves of KEP mice treated with control antibody (Ab) ($n = 20$ animals), anti-CSF-1R ($n = 22$ animals), cisplatin (CIS) + control Ab ($n = 21$ animals) or cisplatin + anti-CSF-1R ($n = 16$ animals). Cisplatin + control Ab versus control Ab: $P = 0.0001$; cisplatin + control Ab versus anti-CSF-1R: $P = 0.0001$; cisplatin + anti-CSF-1R versus cisplatin + control Ab: $P = 0.0011$ (two-tailed log-rank test). **g**, Percentage of non-viable area per tumour section of time-point-sacrificed KEP mice quantified by digital area analysis of H&E-stained sections (control Ab: $n = 5$ animals; anti-CSF-1R: $n = 5$ animals; cisplatin + control Ab: $n = 6$ animals; cisplatin + anti-CSF-1R: $n = 8$ animals). Representative H&E sections are shown, and the dashed line separates the viable from the non-viable area. Scale bars, 50 μm. **h**, Quantification of BrdU$^+$ cells in viable areas of mammary tumours of time-point-sacrificed KEP mice (control Ab: $n = 6$ animals, anti-CSF-1R: $n = 5$ animals, cisplatin + control Ab: $n = 8$ animals, cisplatin + anti-CSF-1R: $n = 9$ animals). The values represent the average number of BrdU$^+$ cells per field of view (FOV) quantified by counting five high-power microscopic fields per tumour. Representative BrdU immunohistochemistry stainings are shown. Scale bars, 25 μm. **i**, Kaplan–Meier tumour-specific survival curves of untreated KEP mice ($n = 12$ animals) or mice treated with oxaliplatin (OX) + control Ab ($n = 10$ animals) and oxaliplatin + anti-CSF-1R ($n = 12$ animals). Oxaliplatin + control Ab versus no treatment: $P = 0.0015$; oxaliplatin + control Ab versus oxaliplatin + anti-CSF-1R: $P = 0.0507$ (two-tailed log-rank test). Data presented in **a**, **d**, **e**, **g** and **h** are mean ± s.e.m., and statistical analysis was performed using the two-tailed Mann–Whitney test.

CSF-1R blockade in tumour-bearing KEP mice enhances the anticancer efficacy of platinum-based chemotherapy

We next tested the anticancer efficacy of anti-CSF-1R in combination with two conventional chemotherapeutics with a different mode of action: cisplatin, a platinum-based anticancer drug that crosslinks DNA and induces apoptosis, and docetaxel, an antimitotic agent that interferes with cell division through stabilization of microtubules. Successful blockade of the CSF-1R pathway during treatment of tumour-bearing KEP mice with chemotherapy and anti-CSF-1R was confirmed by the reduction in the number of TAMs (Fig. 1c,d and Supplementary Fig. 2a,b). Interestingly, anti-CSF-1R synergized with cisplatin, resulting in prolonged survival compared to cisplatin + control antibody-treated mice (Fig. 1f). By contrast, no therapeutic synergy was observed in docetaxel + anti-CSF-1R-treated mice (Supplementary Fig. 2c). The therapeutic synergy observed upon cisplatin + anti-CSF-1R was associated with more necrosis in KEP tumours (Fig. 1g) but not with more cleaved caspase 3$^+$ apoptotic cells (Supplementary Fig. 2d). Perhaps other mechanisms of cell death are involved or the timing of our analysis was suboptimal for this parameter. Furthermore, anti-CSF-1R monotherapy—and to a lesser extent, the combination with cisplatin—decreased the number of BrdU$^+$-proliferating cells (Fig. 1h). No significant changes in the number and pericyte coverage of CD31$^+$ microvessels, the amount of intratumoural DNA double-strand breaks and intratumoural cisplatin-adduct formation were observed at the time-point analysed (Supplementary Fig. 2e–h). As expected, none of these parameters was changed in the docetaxel setting (Supplementary Fig. 2i–m).

To assess whether the anti-CSF-1R-mediated therapeutic synergy was unique to cisplatin or could be extended to drugs with a similar mechanism of action, we tested another platinum-containing drug, oxaliplatin, and also found that the survival benefit of oxaliplatin was improved by combined CSF-1R blockade (Fig. 1i and Supplementary Fig. 2n). These data demonstrate that anti-CSF-1R acts synergistically with platinum-based chemotherapeutic drugs to extend the survival of mammary tumour-bearing KEP mice.

CSF-1R inhibition alters the innate immune landscape of KEP tumours
Macrophages are key orchestrators of the inflammatory TME[28]. Thus, we set out to assess the effect of anti-CSF-1R on the innate immune landscape of KEP tumours. Despite the strong reduction of CD11b$^+$F4/80$^+$ TAMs on anti-CSF-1R, up to 20% of the intratumoural CD45$^+$ immune cells still expresses the macrophage marker F4/80 (Fig. 1d). Detailed analysis of this surviving CD11b$^+$F4/80$^+$ population revealed that an increased proportion of these cells expresses the inflammatory monocyte marker Ly6C compared to CD11b$^+$F4/80$^+$ cells in control antibody-treated tumours (Fig. 2a and Supplementary Fig. 3a). Moreover, the surviving CD11b$^+$F4/80$^+$ cells in cisplatin + anti-CSF-1R-treated tumours express elevated levels of the co-stimulatory molecules CD80 and CD86, slightly elevated MHCII levels, decreased levels of the chemokine receptors C-C chemokine receptor type 2 (CCR2) and CX3C chemokine receptor 1 (CX3CR1), and increased levels of programmed cell death 1 ligand 1 (PD-L1) compared to intratumoural CD11b$^+$F4/80$^+$ cells in cisplatin + control antibody-treated mice (Fig. 2b–g). Furthermore, in the independent orthotopically transplanted *K14cre;Trp53$^{F/F}$* (KP) mammary tumour model, intratumoural CD11b$^+$F4/80$^+$ myeloid cells remaining after CSF-1R inhibition display an altered phenotype corresponding to that in anti-CSF-1R-treated KEP tumours (Fig. 2h–m). Thus, anti-CSF-1R depletes the majority of CD11b$^+$F4/80$^+$ TAMs, whereas a small population of CD11b$^+$F4/80$^+$ cells with a distinct phenotype survives. To explore whether these surviving cells could derive from circulating monocytes, we transferred tdTomato$^+$ monocytes into control antibody or anti-CSF-1R-treated tumour-bearing KEP mice. After 4 d, the transferred monocytes that infiltrated tumours of anti-CSF-1R-treated, and not control antibody-treated, animals partially acquired the phenotype of the surviving intratumoural CD11b$^+$F4/80$^+$ cell population (that is, loss of CX3CR1 and elevated PD-L1 expression) (Supplementary Fig. 3b–d). These findings suggest that the surviving CD11b$^+$F4/80$^+$ cells in anti-CSF-1R-treated tumours may derive from newly recruited circulating monocytes, although other mechanisms cannot be excluded.

Whereas in treatment-naive KEP tumours the macrophage/neutrophil ratio is approximately 3/1, in anti-CSF-1R-treated tumours, either in the presence or absence of cisplatin, this ratio is reversed (Fig. 1d,e). However, the absolute number of intratumoural neutrophils was not increased upon CSF-1R inhibition (Supplementary Fig. 3e). Anti-CSF-1R treatment induced an increase in the number of monocytes and a modest, but not significant, and very variable increase in the number of intratumoural eosinophils and mast cells (Supplementary Fig. 3f–h). Together, these data show that cisplatin + anti-CSF-1R synergy is accompanied by changes in the myeloid immune landscape of tumours. Most notably, anti-CSF-1R treatment resulted in a surviving population of CD11b$^+$F4/80$^+$ cells with an altered
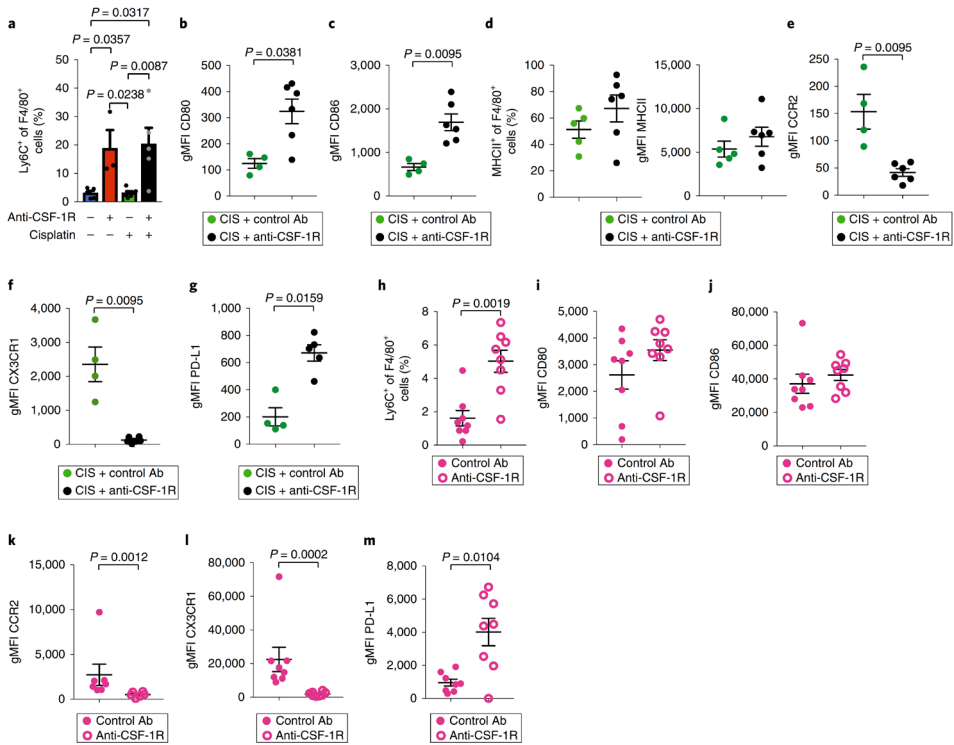
phenotype.

Fig. 2| Characterization of F4/80⁺ cells by flow cytometry in spontaneous KEP tumours and in orthotopically transplanted KP tumours after anti-CSF-1R treatment. a, Percentage of CD11b⁺F4/80⁺ immune cells expressing Ly6C in end-stage KEP tumours (untreated: $n = 5$ animals; anti-CSF-1R: $n = 3$ animals; cisplatin: $n = 6$ animals; cisplatin + anti-CSF-1R: $n = 5$ animals). **b,c**, Geometric mean fluorescence intensity (gMFI) of CD80 (**b**) and CD86 (**c**) expression on F4/80⁺Siglec F⁻ cells in KEP tumours (cisplatin + control Ab: $n = 4$ animals; cisplatin + anti-CSF-1R: $n = 6$ animals). **d**, Percentage of MHCII-expressing F4/80⁺Siglec F⁻ cells (left) and gMFI (right) of MHCII on F4/80⁺Siglec F⁻ in the KEP tumours (cisplatin + control Ab: $n = 5$ animals; cisplatin + anti-CSF-1R: $n = 6$ animals). gMFI was calculated by subtracting the gMFI of the MHCII-negative population from the gMFI of the MHCII-positive population. **e–g**, gMFI of CCR2 (**e**), CX3CR1 (**f**) and PD-L1 (**g**) expression on F4/80⁺Siglec F⁻ cells in KEP tumours (CCR2 and CX3CR1: cisplatin + control Ab: $n = 4$ animals; cisplatin + anti-CSF-1R: $n = 6$ animals; PD-L1: cisplatin + control Ab: $n = 4$ animals; cisplatin + anti-CSF-1R: $n = 5$ animals). **h–m**, KP tumour pieces were orthotopically transplanted in the mammary fat pad of FVB/N mice. The percentage of CD11b⁺F4/80⁺Siglec F⁻ immune cells expressing Ly6C in time-point-sacrificed KP tumours (**h**). gMFI of CD80 (**i**), CD86 (**j**), CCR2 (**k**), CX3CR1 (**l**) and PD-L1 (**m**) expression on F4/80⁺Siglec F⁻ cells in time-point-sacrificed KP tumours ($n = 8$ animals per group, except CCR2: control Ab: $n = 7$ animals, anti-CSF-1R: $n = 6$ animals). The gMFI values presented in **b**, **c**, **e–g** and **i–m** were determined by subtracting the gMFIs of the fluorescence minus one staining from the gMFI of the full staining. Data presented in **a–m** are mean ± s.e.m., and statistical analysis was performed using the two-tailed Mann–Whitney test.

Macrophage blockade enhances cisplatin response by unleashing intratumoural type I IFN signalling

To better characterize the phenotype of the anti-CSF-1R-surviving intratumoural CD11b$^+$F4/80$^+$ cells, next-generation RNA sequencing (RNA-seq) analysis was performed on CD11b$^+$F4/80$^+$ cells sorted from cisplatin + control antibody-treated or cisplatin + anti-CSF-1R-treated tumours. Hierarchical clustering of the top 400 variable genes revealed that CD11b$^+$F4/80$^+$ cells from cisplatin + anti-CSF-1R-treated tumours displayed a different transcriptome profile, mainly characterized by a strong enrichment of genes involved in type I IFN signalling and type I IFN production, whereas cell-cycle-associated genes were reduced (Fig. 3a,b). Interestingly, CSF-1R expression levels were lower in the remaining CD11b$^+$F4/80$^+$ cells from cisplatin + anti-CSF-1R-treated tumours (fold change: −2,04; $P = 3.63 \times 10^{-5}$), perhaps explaining why these cells resisted anti-CSF-1R therapy. In parallel, we also performed RNA-seq on flow-sorted Ly6G$^+$Ly6C^{low} neutrophils isolated from tumours of cisplatin + control antibody-treated and cisplatin + anti-CSF-1R-treated KEP mice. Hierarchical clustering of the top 400 variable genes within this data set revealed that anti-CSF-1R treatment also had a significant effect on the transcriptome profile of tumour-associated neutrophils (Supplementary Fig. 4a). To ensure that these transcriptome alterations in neutrophils are not a direct effect of anti-CSF-1R on neutrophils, but rather an indirect consequence of macrophage targeting, we performed gene set enrichment analysis (GSEA) of target genes of early growth receptor 2 (EGR2), a transcription factor downstream of CSF-1R signalling[29]. No differences were observed in the expression of EGR2 target genes between neutrophils isolated from anti-CSF-1R-treated and control antibody-treated tumours (Supplementary Fig. 4b), suggesting that neutrophils are not directly influenced by anti-CSF-1R. Interestingly, BiNGO analysis of the top 100 upregulated and downregulated genes and Ingenuity pathway analysis of the differentially expressed genes revealed an enrichment in genes involved in type I IFN signalling in neutrophils isolated from cisplatin + anti-CSF-1R-treated tumours versus cisplatin + control antibody-treated tumours (Supplementary Fig. 4c,d and Supplementary Table 3). These data indicate that the therapeutic benefit of cisplatin + anti-CSF-1R is accompanied by induction of type I IFN-stimulated genes (ISGs) in both intratumoural CD11b$^+$F4/80$^+$ cells and neutrophils.

We hypothesized that the enrichment of ISGs in these intratumoural immune populations was a consequence of increased levels of type I IFNs in KEP tumours upon CSF-1R blockade. Indeed, by using primers hybridizing to all *Ifna* genes, mRNA expression of *Ifna*, but not *Ifnb*, was increased in tumours of cisplatin + anti-CSF-1R-treated KEP mice compared to cisplatin + control antibody-treated mice (Fig. 3c). In line with this, the mRNA levels of various intracellular pattern recognition receptors, such as *Tlr3*, *Rig1* and *Ifih1*, whose signals induce type I IFN production, were upregulated in cisplatin + anti-CSF-1R-treated tumours compared to cisplatin + control antibody treatment (Fig. 3d). Notably, the increase in type I IFN expression upon anti-CSF-1R was independent of chemotherapy treatment, as a similar intratumoural increase in *Ifna* expression was observed upon anti-CSF-1R alone (Fig. 3e) or with docetaxel + anti-CSF-1R (Supplementary Fig. 5a). We also confirmed the increased expression of *Ifna*—and of two ISGs, *Isg15* and *Oas1a*—

5

upon anti-CSF-1R treatment in the independent KP-based tumour transplantation model and in inoculated MC38 colorectal adenocarcinoma tumours[21] (Fig. 3f,g and Supplementary Fig. 5b,c). Together, these data demonstrate that anti-CSF-1R induces type I IFN in the TME.
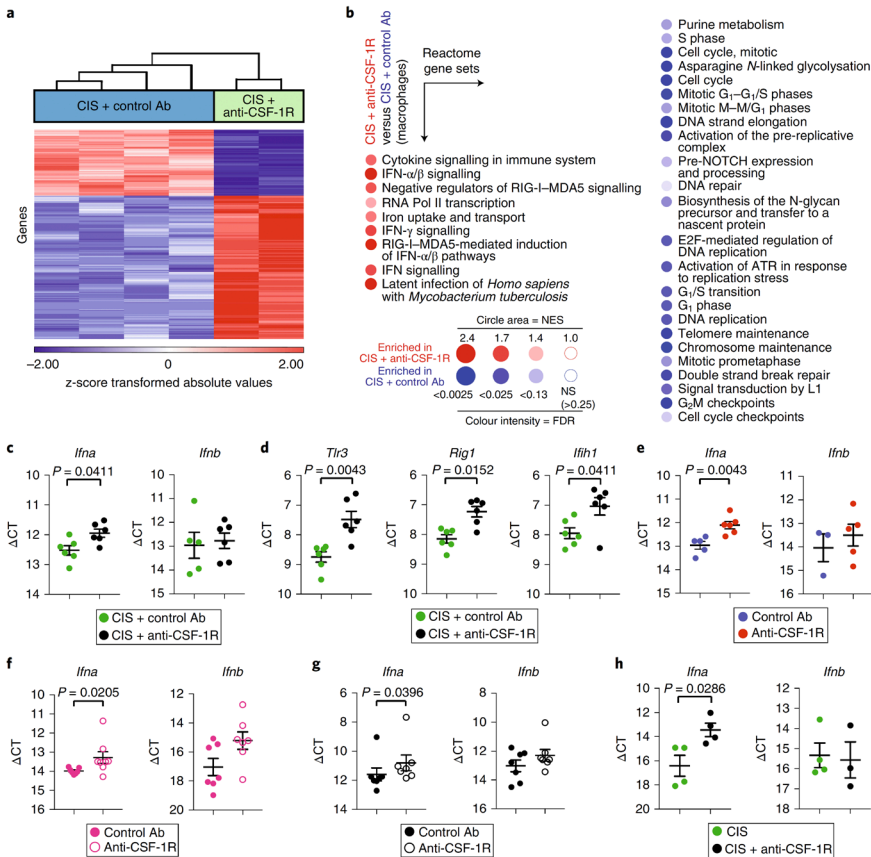

Fig. 3 | CSF-1R inhibition alters TAM phenotype and induces type I IFN signalling in the TME. a, Hierarchical clustering of the top 400 variable genes between CD11b⁺F4/80⁺ cells isolated from KEP tumours treated with cisplatin + control Ab ($n = 4$ animals) and cisplatin + anti-CSF-1R ($n = 2$ biologically independent samples, a pool of five mice each). Fold change ≥ 1.5; P value with FDR correction ≤ 0.05. Statistical analysis was performed using two-way ANOVA. **b**, BubbleGUM visualization of GSEA using reactome gene sets comparing CD11b⁺F4/80⁺ cells from cisplatin + anti-CSF-1R-treated tumours versus macrophages from cisplatin + control Ab-treated tumours. Same mice as in **a**. Normalized enrichment score (NES) ≥ 1, FDR value: ≤0.25. The enrichment score was calculated using a weighted Kolmogorov–Smirnov-like statistic. MDA5, melanoma differentiation-associated protein 5 (encoded by *Ifih1*); Pol, polymerase; RIG-I, retinoic acid inducible gene I; ATR, ATM and Rad3-related; NS, not significant. **c**, Transcripts of *Ifna* ($n = 6$ animals per group) and *Ifnb* ($n = 5$ animals in cisplatin + control Ab; $n = 6$ animals in cisplatin + anti-CSF-1R). **d**, *Tlr3*, *Rig1* and *Ifih1* in KEP mammary tumours isolated 1 d after the second cisplatin injection were determined by quantitative PCR and normalized to β-actin ($n = 6$ animals per group). **e–g**, Transcripts of *Ifna* and *Ifnb* in KEP mammary tumours (*Ifna*: $n = 5$ animals in control Ab, $n = 6$ animals in anti-CSF-1R; *Ifnb*: $n = 3$ animals in control Ab, $n = 5$ animals in anti-CSF-1R) (**e**), orthotopically transplanted KP mammary tumour (*Ifna*: $n = 7$ animals in control Ab, $n = 8$ animals in anti-CSF-1R; *Ifnb*: $n = 7$ animals per group) (**f**) and subcutaneously inoculated MC38 tumours ($n = 7$ animals per group) (**g**) treated with control Ab and anti-CSF-1R were determined by quantitative PCR

and normalized to β-actin. Mice were analysed at a tumour size of 100 mm² (KP) or after 12 d from the start of the treatment (MC38). **h**, Transcripts of *Ifna* ($n = 4$ animals per group) and *Ifnb* ($n = 4$ animals in cisplatin, $n = 3$ animals in cisplatin + anti-CSF-1R) in CD11b⁺F4/80⁺ cells isolated from end-stage KEP tumours were determined by quantitative PCR and normalized to β-actin. Graphs in **c–h** show the mean ± s.e.m. in ΔCT values, and statistical analysis was performed using the two-tailed Mann–Whitney test.

To pursue the cellular source of type I IFN, we flow-sorted different cell populations from cisplatin and cisplatin + anti-CSF-1R-treated KEP tumours (Supplementary Fig. 5d) and compared *Ifna* and *Ifnb* transcript levels. Plasmacytoid dendritic cells are known for their ability to produce type I IFN; however, as very few plasmacytoid dendritic cells—less than 0.1% of the total intratumoural immune population—are present in KEP tumours (Supplementary Fig. 5e,f), we could not recover RNA of sufficient quality. Likewise, we did not obtain RNA of sufficient quality from sorted CD31⁺ endothelial cells. Only the CD11b⁺F4/80⁺ immune cell population displayed elevated *Ifna* expression levels upon CSF-1R blockade (Fig. 3h and Supplementary Fig. 5g,h). In line with these in vivo findings, in vitro treatment of bone marrow-derived macrophages (BMDMs) with anti-CSF-1R modestly induces *Ifna* levels after 24 h of culture (Supplementary Fig. 5i). These analyses suggest that the surviving population of intratumoural CD11b⁺F4/80⁺ cells is an important source of IFN-α in cisplatin + anti-CSF-1R-treated KEP tumours.

To dissect the functional significance of type I IFN signalling in the therapeutic benefit of cisplatin + anti-CSF-1R therapy, we blocked the IFN-α/β receptor subunit 1 (IFNAR1) in KEP mice. Whereas blockade of type I IFN signalling did not influence the anticancer efficacy of cisplatin, anti-IFNAR1 treatment completely abrogated the synergistic effect of cisplatin + anti-CSF-1R treatment (Fig. 4a). These findings reveal that therapeutic targeting of macrophages with anti-CSF-1R in tumour-bearing KEP mice unleashes intratumoural type I IFN signalling, which enhances the therapeutic efficacy of cisplatin.

Emactuzumab treatment induces intratumoural type I ISGs in patients with cancer
To validate our preclinical findings that CSF-1R blockade unleashes intratumoural type I IFN signalling in patients, we compared ISG expression levels in pre-treatment and on-treatment tumour biopsies from patients with advanced solid tumours treated with emactuzumab (RG7155), a humanized anti-human CSF-1R monoclonal antibody (NCT01494688)[21,30]. Gene expression profiling was performed on tumour biopsies taken before the start of treatment and after 4 weeks of emactuzumab therapy. We assessed the expression level of a set of 28 ISGs that was selected based on the RNA-seq results from our KEP mouse model (Fig. 3a, Supplementary Fig. 4a,c,d and Supplementary Table 3). The intratumoural expression of all 28 selected ISGs was increased in emactuzumab on-treatment biopsies versus pre-treatment biopsies, of which 11 ISGs were significantly upregulated (Fig. 4b,c). Thus, in line with our preclinical studies, these clinical findings indicate that CSF-1R blockade is a powerful strategy to augment intratumoural type I IFN signalling.

5
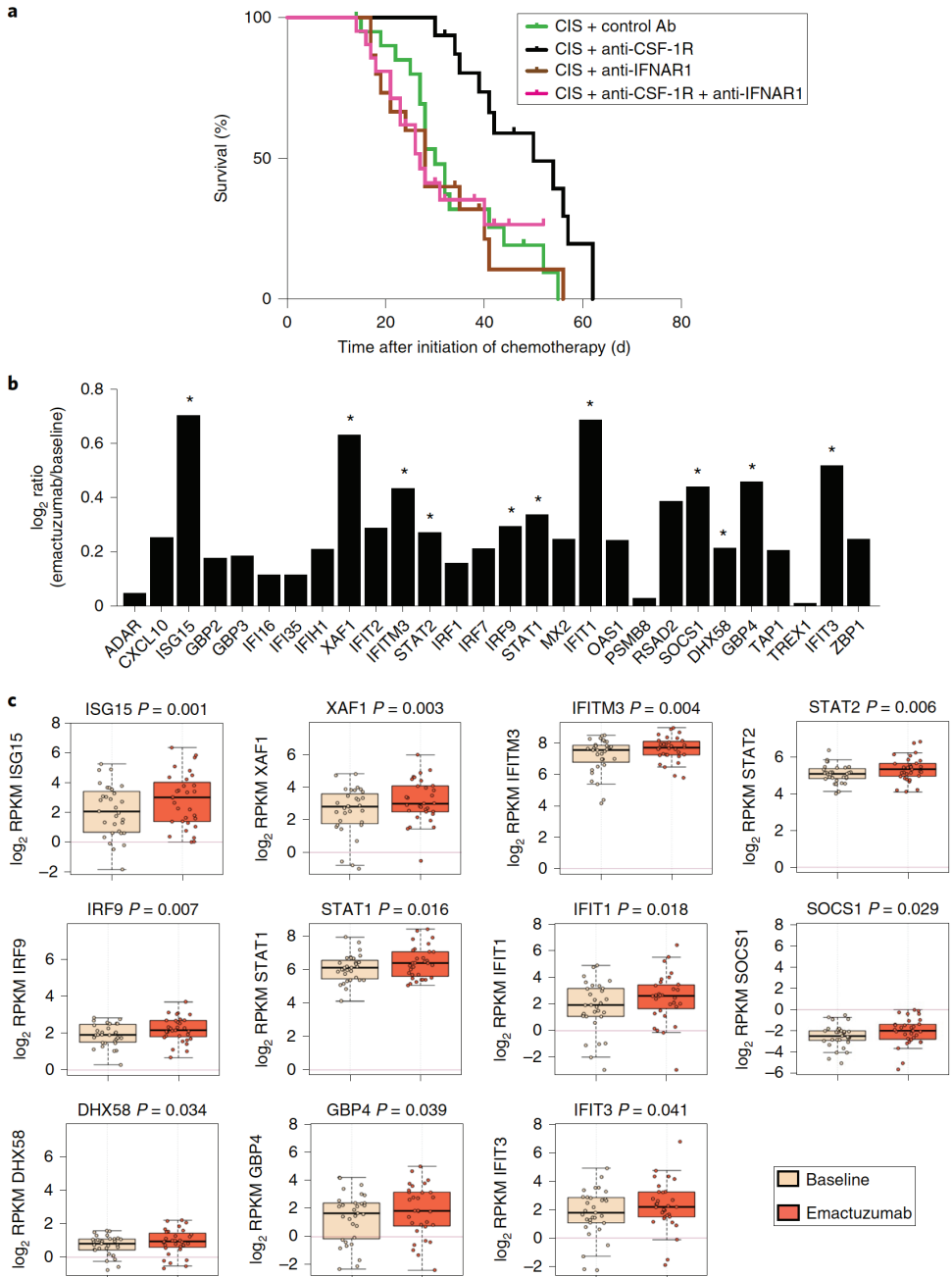
Fig. 4 | CSF-1R blockade increases the expression of intratumoural type I IFN signalling in patients with cancer treated with emactuzumab and is essential for the therapeutic synergy of cisplatin + anti-CSF-1R in the KEP mouse model. a, Kaplan–Meier tumour-specific survival curves of KEP mice treated with cisplatin + control Ab, cisplatin + anti-CSF-1R (same groups as in Fig. 1f), cisplatin + anti-IFNAR1 ($n = 15$ animals) or cisplatin + anti-CSF-1R + anti-IFNAR1 ($n = 21$ animals). Cisplatin + anti-CSF-1R versus cisplatin + anti-CSF-1R + anti-IFNAR1: $P = 0.0064$ (two-tailed log-rank test). **b**, $\log_2$ ratio of

intratumoural expression levels of 28 type I ISGs in emactuzumab (anti-CSF-1R)-treated patients (n = 31 patients) normalized against the pre-treatment expression levels. **c**, Box plots of the expression level of the 11 statistically significant upregulated type I ISGs in tumours of emactuzumab-treated patients (data from **b**, indicated by asterisks). Expression levels in the pre-treatment (baseline) tumour biopsies are compared to on-treatment (emactuzumab) biopsies. The top-most line is the maximum, the top of the box is the third quartile, the centre line is the median, the bottom of the box is the first quartile and the bottom-most line is the minimum. RPKM, reads per kilobase of exon per million mapped reads. The P values were determined by a two-tailed Student's t-test.

Combined CSF-1R inhibition and neutrophil depletion engages antitumour immunity that further improves the therapeutic benefit of cisplatin

Type I IFNs are emerging as key regulators of cancer growth and therapy response[31,32]. Type I IFNs can affect cancer biology via different mechanisms, including the induction of anti-proliferative and pro-apoptotic effects on IFNAR+ cancer cells[33,34]. Indeed, exposure of a cell line derived from a spontaneous KEP mammary tumour to recombinant IFN-α1 results in a dose-dependent decrease in colony-forming ability, also in combination with cisplatin, suggesting that type I IFNs have a direct inhibitory effect on KEP cancer cells (Fig. 5). Because type I IFNs are also key orchestrators of antitumour immunity[33,34,35], we hypothesized that the anti-CSF-1R-induced type I IFN-enriched TME may foster antitumour CD8+ T cell activity. However, we observed fewer numbers of tumour-infiltrating CD4+ or CD8+ T cells in cisplatin + anti-CSF-1R-treated tumours than in cisplatin + control antibody-treated tumours (Supplementary Fig. 6a–c), and the CD8/regulatory T cell ratio was not affected (Fig. 6a). More natural killer (NK) cells were infiltrating the cisplatin + anti-CSF-1R-treated KEP tumours; however, the number of granzyme B+ cells was not affected compared to cisplatin + control antibody treatment (Fig. 6b,c and Supplementary Fig. 6d). We previously reported that cisplatin efficacy is independent of the adaptive immune system[3], and, in line with the lack of more intratumoural granzyme B+ cells and T cells, here, we also show that antibody-mediated depletion of CD8+ T cells does not reduce the therapeutic efficacy of cisplatin + anti-CSF-1R therapy (Fig. 6d). In addition, genetic ablation of the entire adaptive immune system by crossing KEP mice with *Rag1*^{−/−} mice did not affect therapeutic synergy (Fig. 6g). These data indicate that the anti-CSF-1R-mediated conversion of the TME into a type I IFN-enriched milieu in cisplatin-treated mice is not sufficient to successfully engage an endogenous antitumour T cell response.
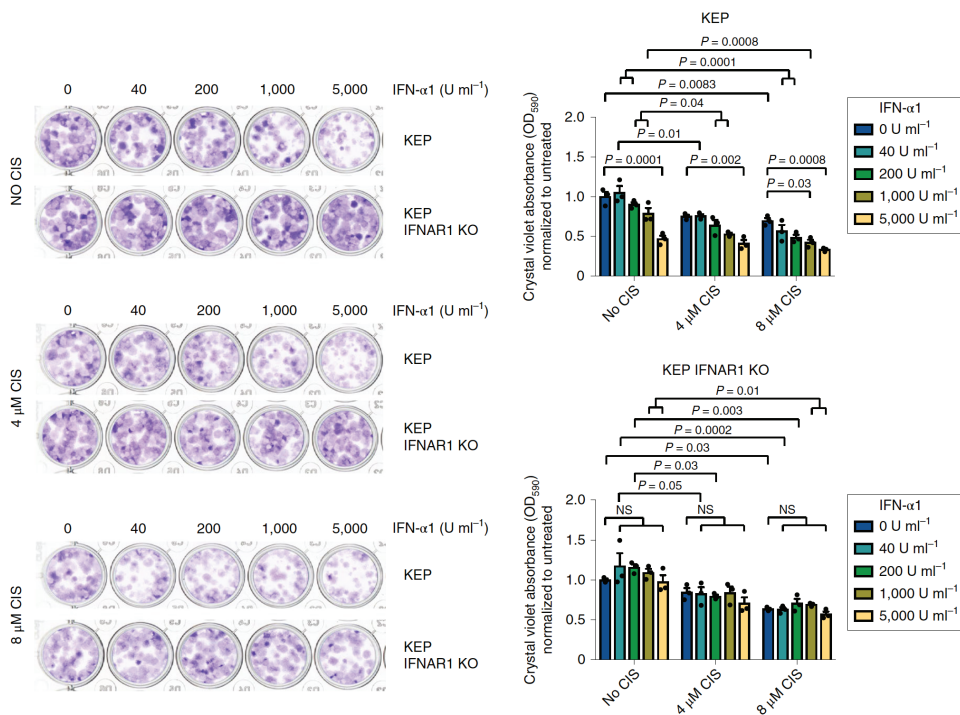
5

Fig. 5 | Direct inhibitory effect of IFN-α1 on a KEP-derived cancer cell line. Representative images of a colony-forming assay with KEP-derived cancer cells and IFNAR1 KO KEP cancer cells treated with increasing concentrations of IFN-α1 and cisplatin. After 7 d, crystal violet was dissolved and absorbance was measured at 590 nm. Data are representative of three independent experiments. Data are mean ± s.e.m. The P value was determined by two-way ANOVA with Tukey's multiple comparison test.

We next hypothesized that it may be necessary to breach an additional layer of immunosuppression before antitumour immunity can be unleashed. The most abundant immune cell population in cisplatin + anti-CSF-1R-treated KEP tumours is neutrophils (Fig. 1e) and we have previously reported that KEP tumour-educated neutrophils are very immunosuppressive[36]. To address whether neutrophils impede antitumour immunity in cisplatin + anti-CSF-1R-treated mice, we treated tumour-bearing KEP mice with the neutrophil-specific anti-Ly6G antibody (clone 1A8). Immunohistochemistry for S100A9 confirmed a reduction in the number of neutrophils in the lungs and to a lesser extent in the tumour (Supplementary Fig. 6e,f). Cisplatin + anti-CSF-1R + anti-Ly6G treatment significantly improved tumour control and prolonged the survival of KEP mice compared to cisplatin + anti-CSF-1R therapy (Fig. 6e). Whereas cisplatin + anti-CSF-1R temporarily stabilizes tumour outgrowth, we observed tumour shrinkage in six out of ten mice treated with cisplatin + anti-CSF-1R + anti-Ly6G, and the mammary tumours of two of these mice regressed completely during treatment (Supplementary Fig. 6g,h). Anti-Ly6G treatment alone failed to influence primary tumour growth in KEP mice

as previously shown[36], neither did the combination of anti-CSF-1R + anti-Ly6G (Supplementary Fig. 6i) nor did anti-Ly6G alter the efficacy of cisplatin (Fig. 6e). Further characterization of cisplatin + anti-CSF-1R + anti-Ly6G-treated KEP tumours showed a significant reduction in the number of BrdU$^+$-proliferating cells and γ-H2AX$^+$ DNA-damaged cells (Supplementary Fig. 6j,k). No statistically significant differences were observed in the number of apoptotic cells, CD31$^+$ vessels and cisplatin adducts (Supplementary Fig. 6l–n). Interestingly, the CD8/regulatory T cell ratio, the absolute number of NK cells and the absolute and relative number of granzyme B$^+$ immune cells were increased in cisplatin + anti-CSF-1R + anti-Ly6G-treated tumours compared to cisplatin + control antibody therapy (Fig. 6a–c and Supplementary Fig. 6d). Importantly, the additional therapeutic benefit obtained by anti-Ly6G treatment was partially lost after antibody-mediated depletion of CD8$^+$ T cells or NK cells (Fig. 6e,f) and was completely abrogated when the same treatment was performed in KEP;*Rag1*$^{-/-}$ mice (Fig. 6g). Collectively, these data indicate that the combined anti-CSF-1R-mediated conversion of the tumour milieu into a type I IFN-enriched environment and the relieve of neutrophil-dependent immunosuppression fosters engagement of antitumour immunity in the anticancer effect of cisplatin in this poorly immunogenic mouse tumour model.
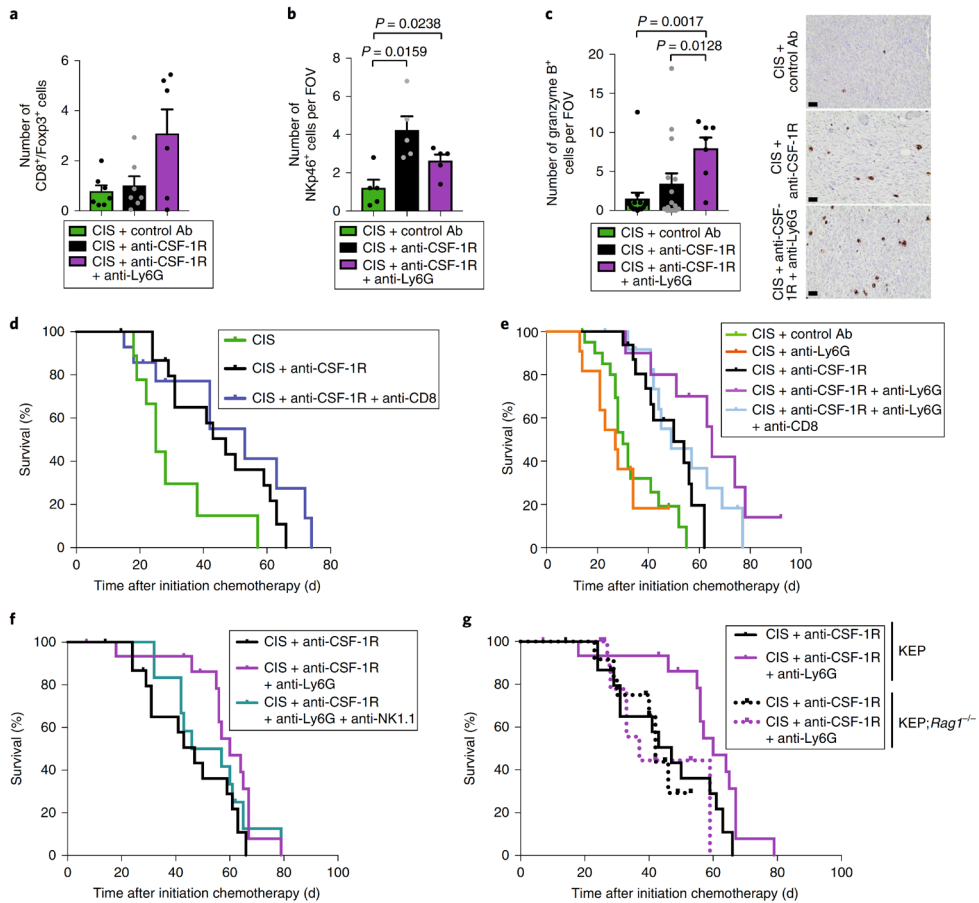
5

Fig. 6 | Neutrophil inhibition engages antitumour immunity and further improves cisplatin + anti-CSF-1R efficacy. a, CD8^{+} T cell/Foxp3^{+} T cell ratio based on immunohistochemistry staining in the tumour of time-point-sacrificed KEP mice (cisplatin + control Ab and cisplatin + anti-CSF-1R: $n = 7$ animals; cisplatin + anti-CSF-1R + anti-Ly6G: $n = 6$ animals). **b,c**, Quantification of NKp46^{+} cells (**b**) and granzyme B^{+} cells (**c**) in viable areas of mammary tumours of time-point-sacrificed KEP mice treated with cisplatin + control Ab (NKp46: $n = 5$ animals; granzyme B: $n = 15$ animals), cisplatin + anti-CSF-1R (NKp46: $n = 5$ animals; granzyme B: $n = 15$ animals) and cisplatin + anti-CSF-1R + anti-Ly6G (NKp46: $n = 5$ animals; granzyme B: $n = 7$ animals). The values represent the average number of positive cells per FOV quantified by counting five high-power microscopic fields per tumour. Representative granzyme B immunohistochemistry stainings are shown (**c**). Scale bars, 50 μm. **d**, Kaplan–Meier tumour-specific survival curves of KEP mice treated with cisplatin + control Ab ($n = 6$ animals), cisplatin + anti-CSF-1R ($n = 16$ animals) and cisplatin + anti-CSF-1R + anti-CD8 ($n = 14$ animals). Cisplatin + anti-CSF-1R + anti-CD8-treated mice versus cisplatin + anti-CSF-1R-treated mice: $P = 0.3728$ (two-tailed log-rank test). **e**, Kaplan–Meier tumour-specific survival curves of KEP mice treated with cisplatin + control Ab, cisplatin + anti-CSF-1R (same groups as in Fig. 1f), cisplatin + anti-Ly6G ($n = 11$ animals), cisplatin + anti-CSF-1R + anti-Ly6G ($n = 10$ animals) or cisplatin + anti-CSF-1R + anti-Ly6G + anti-CD8 ($n = 13$ animals). Cisplatin + anti-CSF-1R-treated mice versus cisplatin + anti-CSF-1R + anti-Ly6G-treated mice: $P = 0.0085$; cisplatin + anti-CSF-1R-treated mice versus cisplatin + anti-CSF-1R + anti-Ly6G + anti-CD8-treated mice: $P = 0.1104$ (two-tailed log-rank test). **f**, Kaplan–Meier tumour-specific survival curves of KEP mice treated with cisplatin + anti-CSF-1R ($n = 16$ animals, same curve as in **d**), cisplatin + anti-CSF-1R + anti-Ly6G ($n = 17$ animals of which 4 mice were treated with cisplatin + anti-CSF-1R + anti-Ly6G + IgG2a; no differences were observed between cisplatin + anti-CSF-1R + anti-Ly6G

and cisplatin + anti-CSF-1R + anti-Ly6G + IgG2a), or cisplatin + anti-CSF-1R + anti-Ly6G + anti-NK1.1 ($n = 12$ animals). Cisplatin + anti-CSF-1R-treated mice versus cisplatin + anti-CSF-1R + anti-Ly6G-treated mice: $P = 0.0226$; cisplatin + anti-CSF-1R-treated mice versus cisplatin + anti-CSF-1R + anti-Ly6G + anti-NK1.1-treated mice: $P = 0.4073$ (two-tailed log-rank test). **g**, Kaplan–Meier tumour-specific survival curves comparing cisplatin + anti-CSF-1R and cisplatin + anti-CSF-1R + anti-Ly6G treatment in KEP (same as in **f**) and KEP;$Rag1^{-/-}$ mice. Cisplatin + anti-CSF-1R in KEP;$Rag1^{-/-}$ ($n = 12$ animals) and cisplatin + anti-CSF-1R + anti-Ly6G in KEP;$Rag1^{-/-}$ ($n = 11$ animals). Cisplatin + anti-CSF-1R + anti-Ly6G-treated KEP;$Rag1^{-/-}$ mice versus cisplatin + anti-CSF-1R-treated KEP;$Rag1^{-/-}$ mice: $P = 0.9597$ (two-tailed log-rank test). Data presented in **a–c** are mean ± s.e.m., and statistical analysis was performed using the two-tailed Mann–Whitney test.

Discussion

There is a growing realization that immune-mediated mechanisms influence the responsiveness of tumours to chemotherapy[1]. Notably, macrophages actively interfere with the therapeutic efficacy of chemotherapy via several mechanisms in mouse tumour models, including suppression of antitumour immunity through IL-10 secretion[5], secretion of chemoprotective proteases such as cathepsins[12] or secretion of lysophospholipids[15] that interfere with the DNA damage response. These macrophage-mediated chemotherapy resistance mechanisms are dependent on the production of soluble mediators from TAMs. Our study reveals a conceptually different mechanism of how therapeutic targeting of macrophages improves chemotherapy efficacy. Through in vivo mechanistic studies in the KEP transgenic mouse model for breast cancer, we demonstrate that macrophage inhibition with anti-CSF-1R induces intratumoural type I IFN signalling, which acts synergistically with cisplatin to inhibit tumour outgrowth and extend survival.

There is a growing interest in the effect of type I IFNs on cancer behaviour and response to immune checkpoint inhibitors, radiotherapy and chemotherapy[32,37,38,39]. Besides being associated with an improved prognosis[40,41,42], an intratumoural IFN signature in patients with breast cancer has been correlated with improved chemotherapy response[37], and preclinical studies reported that type I IFN enhanced chemotherapy efficacy[37,43]. However, IFN-related gene signatures have also been correlated with chemotherapy resistance[44], consistent with a pleomorphic and still poorly understood role of type I IFN signalling in the tumour context. Importantly, impaired type I IFN signalling is a prominent feature of immune dysfunction in patients with cancer[45]. Our study reveals that anti-CSF-1R represents a powerful approach to induce intratumoural IFN signalling and to sensitize tumours to cisplatin. Notably, we find that anti-CSF-1R treatment in patients with cancer also results in increased intratumoural expression of ISGs, confirming our findings that anti-CSF-1R unleashes type I IFN response in tumours.

Our study shows that anti-CSF-1R depletes the majority of F4/80+ TAMs; however, a small intratumoural CD11b+F4/80+ population with a distinct phenotype survives. Interestingly, these surviving cells express lower levels of *Csf1r* and significantly higher *Ifna* mRNA levels than the CD11b+F4/80+ cells in untreated tumours, probably accounting for the increased *Ifna* levels in the tumours. A shift in

5

macrophage phenotype was also observed in pancreatic cancer and glioblastoma models upon interference with the CSF-1–CSF-1R pathway[46,47,48,49]. Similar to our model, targeting CSF-1 in the pancreatic cancer models on the one hand depleted TAMs and on the other hand reprogrammed the remaining macrophages to an antitumour phenotype. Interestingly, type I IFN was also found to be increased in these macrophages[49]; however, its effect was not functionally pursued in this study. These data, combined with our observation that IFN-α is also upregulated in anti-CSF-1R-treated MC38 colon adenocarcinoma tumours, indicate that anti-CSF-1R-mediated induction of type I IFNs is not limited to breast cancer, but extends to other cancer types.

Type I IFNs can directly affect cancer cells by inducing apoptosis or blocking proliferation, or indirectly by stimulating antitumour immune responses or inhibiting angiogenesis[33]. In line with the observed in vivo reduction of proliferating tumour cells upon anti-CSF-1R therapy, our in vitro studies indicate that IFN-α1 can directly suppress KEP cancer cells. We did not observe an effect of CSF-1R inhibition on the number of intratumoural blood vessels or their pericyte coverage, excluding an angiogenesis effect. Despite a key role for type I IFNs in dictating antitumour immunity[31,32], the increase in the number of intratumoural type I IFNs was not sufficient to induce effective antitumour T cell responses. In line with the immunosuppressive phenotype of tumour-educated neutrophils in KEP mice[36] and in other models[50], the additional ablation of neutrophils stimulated antitumour immunity. It may be surprising that we observed a therapeutic benefit of depletion of neutrophils with an IFN gene signature in cisplatin + anti-CSF-1R-treated KEP mice, whereas some studies have suggested that type I IFNs can induce antitumour properties in neutrophils[51]. However, in line with our data, a type I IFN transcriptional signature in neutrophils in malaria-infected hosts and in patients with active tuberculosis correlated with tissue damage and disease pathogenesis[52,53], suggesting that, in these settings, type I IFN signalling in neutrophils may contribute to their harmful actions. In addition, although type I IFNs are often considered to exert antitumour functions, several studies on chronic viral infections show negative-feedback mechanisms when persistently present in the environment by, for example, generating an immunosuppressive milieu[34,54,55]. Perhaps in our study a similar mechanism is involved, explaining why the cytotoxic activity of platinum-based chemotherapy is enhanced by type I IFNs, but at the same time, this therapeutic synergy is limited by an immunosuppressive programme. Although T cell activation was implicated in controlling tumour growth upon combined macrophage and neutrophil depletion in a mouse model for pancreatic cancer[20], the full mechanism in the context of chemotherapy was not completely resolved. Our in vivo data demonstrate that, although the release of type I IFN is necessary for cisplatin + anti-CSF-1R therapeutic synergy, it takes further depletion of neutrophils to engage an antitumour immune response during cisplatin treatment.

Interestingly, the platinum-based drugs cisplatin and oxaliplatin synergized with anti-CSF-1R treatment, whereas docetaxel did not, despite the induction of IFN-α in the docetaxel setting. It will be important to mechanistically understand how the type of chemotherapy dictates its ability to act in synergy with type I IFN signalling. These

insights will facilitate the development of optimal combination therapies of CSF-1R-targeting drugs or other type I IFN-inducing agents, including STING (stimulator of IFN genes) agonists[56], with chemotherapeutic agents. To maximize the therapeutic benefit of cytotoxic therapy in poorly immunogenic tumour types, it will be critical to simultaneously target neutrophil-dependent immunosuppression.

Methods

Mice

The generation and characterization of KEP mice have been previously described[24] and are commercially available via Taconic Biosciences. KEP mice were back-crossed onto the FVB/N background, and genotyping was performed by PCR analysis on tail-tip DNA as described[24,36]. KEP mice were crossed with $Rag1^{-/-}$ mice (FVB/N, a gift from L. Coussens, Oregon Health & Science University, Portland) to generate KEP;$Rag1^{-/-}$ mice[3]. Female KEP and KEP;$Rag1^{-/-}$ mice were monitored twice weekly for the spontaneous onset of mammary tumour formation by palpation starting at 4 months of age. Donor tumours from KEP and KP[24] mice were collected in ice-cold PBS, cut into small pieces and resuspended in DMEM F12 containing 30% FCS and 10% dimethyl sulfoxide and stored at −150 °C. The perpendicular tumour diameters of mammary tumours were measured twice a week using a caliper. Age-matched wild-type littermates were used as controls. Female FVB/N mice (10–12 weeks of age) were obtained from Charles River. mTmG mice[57] (back-crossed to the FVB/N background) express tdTomato ubiquitously and were used for the isolation of bone marrow monocytes. Mice were kept in individually ventilated cages at the animal laboratory facility of the Netherlands Cancer Institute (NKI; Amsterdam, the Netherlands). Food and water were provided ad libitum. Animal experiments were approved by the Animal Ethics Committee of the NKI and performed in accordance with institutional, national and European guidelines for animal care and use. The study is compliant with all relevant ethical regulations regarding animal research.

In vivo intervention studies

KEP mice bearing spontaneous mammary tumours were randomized over the treatment groups before initiation of the treatment. Mice were injected intraperitoneally with the chimeric (hamster/mouse) anti-CSF-1R antibody (clone 2G2, Roche Innovation Center Munich; single loading dose of 60 mg per kg followed by 30 mg per kg once a week); control antibody (IgG1, MOPC21, Roche Innovation Center Munich; single loading dose of 60 mg per kg followed by 30 mg per kg once a week); anti-Ly6G antibody (1A8, BioXCell; single loading dose of 400 μg followed by 100 μg three times a week); anti-IFNAR1 (MAR1-5A3, BioXCell; 100 μg three times a week); anti-CD8 (2.43, BioXCell; single loading dose of 400 μg followed by 100 μg three times a week); anti-NK1.1 (PK136, BioXCell; single loading dose of 400 μg followed by 100 μg three times a week); and IgG2a (C1.18.4, BioXCell; single loading dose of 400 μg followed by 100 μg three times a week). The maximum tolerated dose (MTD) dose of cisplatin (5 mg per kg; Accord Healthcare Limited) was administered intravenously every other week for a total of four cycles. The MTD dose of docetaxel (15 mg per kg; Accord Healthcare Limited) was administered

intravenously every week for a total of four cycles. The MTD dose of oxaliplatin (6 mg per kg diluted in NaCl; Fresenius Kabi) was administered intravenously every 10 days for three cycles.

Anti-CSF-1R, control antibodies, anti-Ly6G, anti-CD8 and anti-NK1.1 treatment started when mammary tumours reached a size of $25\,mm^2$; and anti-IFNAR1, cisplatin, docetaxel and oxaliplatin treatment started when mammary tumours reached a size of $50\,mm^2$. For survival curve experiments and end-stage analyses, antibody treatment continued until the tumour or the cumulative tumour burden reached a size of $225\,mm^2$. For survival curve experiments, an event is defined as an animal with a cumulative tumour size of $225\,mm^2$. The main cause of death of censored mice was ulcerated tumours or cisplatin-induced renal toxicity for cisplatin-treated mice.

For time-point analyses, mice were killed 1 d after the second chemotherapy injection (therapy-responsive phase) or at a tumour size of $100\,mm^2$ in chemotherapy-naive mice. To assess tumour cell proliferation, BrdU (50 mg per kg) was injected intraperitoneally into mice 90 min before being sacrificed.

KP tumour pieces were orthotopically transplanted into the mammary fat pad of 10–12-week-old FVB/N female mice. Before initiation of the treatment, mice were randomized over the experimental groups and treated either with control antibody or anti-CSF-1R as described above. Treatment started at a tumour size of $25\,mm^2$ and continued until the tumour reached a size of $100\,mm^2$ when the mice were sacrificed.

MC38 tumours were provided by Roche Innovation Center Munich. MC38 cells were subcutaneously injected into C57Bl6/N mice and, when the tumour volume reached $100\,mm^3$, treated with either control antibody or anti-CSF-1R as described above. Mice were sacrificed 5 d after the second treatment[21].

Intervention studies in the KEP-based spontaneous metastasis model
The orthotopic KEP-based spontaneous metastasis model was described previously in detail[27]. Briefly, KEP tumour pieces ($1 \times 1\,mm$) were orthotopically transplanted into 10–12-week-old FVB/N female mice. Mammary tumours were surgically removed once they reached a tumour size of $225\,mm^2$, after which mice were monitored and sacrificed when they reached the humane end point due to clinically overt metastatic disease. Tumour-bearing recipient mice were treated either with control antibody or with anti-CSF-1R once the mammary tumours reached $5\,mm^2$ (continuous setting) or 3 d after mastectomy (adjuvant setting). Antibody treatment continued until recipient mice developed clinical signs of distress caused by metastatic disease (for example, respiratory distress).

Histology, immunohistochemistry, immunofluorescence and RNA in situ hybridization

All histochemical and immunohistochemical analyses, except NKp46 immunohistochemistry, were performed by the Animal Pathology facility at the NKI. NKp46 immunohistochemistry was performed at the Histology core facility within the Cancer Research UK Beatson Institute (Glasgow, UK). For histochemical analysis, formalin-fixed tissues were processed, sectioned and stained as described[27]. Briefly, tissues were fixed for 24 h in 10% neutral-buffered formalin, embedded in paraffin, sectioned at 4 μm and stained with haematoxylin and eosin (H&E) for histopathological evaluation. H&E slides were digitally processed using the Aperio ScanScope (Aperio). For the quantitative assessment of areas in the tumour that had lost viability, slides were analysed with ImageJ by quantifying the percentage of non-viable areas (defined as areas that lost cellularity) over the total tumour area. Histochemistry for mast cells was performed with Toluidine blue.

For immunohistochemical analysis, paraffin sections were cut and deparaffinized. Antibodies and antigen retrieval methods are described in Supplementary Table 1. Cisplatin adduct staining was performed on frozen tissues embedded in OCT. Quantification of positive cells was performed manually by counting five high-power (40×) fields of view (FOVs) per tumour by two independent operators in a blinded manner. Samples were visualized with a BX43 upright microscope (Olympus) and images were acquired in bright field using cellSens Entry software (Olympus).

The percentages of metastasis-bearing spontaneous KEP mice were calculated based on the microscopic presence or absence of metastatic nodules in lungs and lymph nodes. In the metastasis model, the number of metastatic nodules in the lungs was based on cytokeratin 8 expression. Mice that developed overt metastatic disease were included in the analysis, and mice that were sacrificed because of local recurrence of the primary tumour were excluded.

Immunohistochemistry analysis for CD68 expression (1:2,000, clone KP1, Dako) was performed by the NKI-AvL Core Facility Molecular Pathology and Biobanking on formalin-fixed paraffin-embedded material of ILC breast cancer patients from the RATHER cohort[58,59] enrolled at the NKI. Anonymized archival tissue was used according to national guidelines regarding the use of archival material and with approval of the NKI-AVL translational research board.

Immunofluorescence analysis was performed on formalin-fixed paraffin-embedded material. The list of primary and secondary antibodies is provided in Supplementary Table 1. Sections were counterstained with DAPI (4,6-diamidino-2-phenylindole) and visualized with a Leica SP5 confocal microscope. Images were taken with LAS AF software (Leica) and values were obtained by counting α-SMA$^+$CD31$^+$ cells and total CD31$^+$ cells in six fields per tumour by two independent researches.
I
n situ detection of *Csf1* mRNA was performed using the RNAscope 2.0 FFPE Assay (Advanced Cell Diagnostics) and performed according to the manufacturer's recommendations[60].

Flow cytometry

KEP tumours were collected in ice-cold PBS and processed as described[61]. Briefly, samples were mechanically chopped using the McIlwain tissue chopper (Mickle Laboratory Engineering) and enzymatically digested with 3 mg ml^{-1} collagenase type A (Roche) and 25 µg ml^{-1} DNase I (Sigma) in serum-free medium for 1 h at 37°C in a shaking water bath. After washing, cells were stained with fluorochrome-conjugated antibodies (Supplementary Table 1). For intracellular staining of granzyme B, single-cell suspensions were stimulated in IMDM containing 8% FCS, 100 IU ml^{-1} penicillin, 100 µg ml^{-1} streptomycin, 0.5% β-mercaptoethanol, 50 ng ml^{-1} PMA, 1 µM ionomycin and Golgi-Plug (1:1,000; BD Biosciences) for 3 h at 37 °C. Following surface antigen staining, samples were fixed and permeabilized (BD Biosciences) and stained for intracellular proteins. Data acquisition was performed on BD LSRII or BD LSRFortessa flow cytometer using DIVA software (BD Biosciences) and data analysis was performed using FlowJo software version 9.9.6.

Isolation of intratumoural cell populations

Primary mammary tumours were harvested from KEP mice 1 d after two cycles of chemotherapy (±100 mm^2) or at end-stage (±225 mm^2), and single-cell suspensions were generated as described above. Enrichment of CD11b$^+$ cells was performed using magnetic columns (Miltenyi Biotec), as described previously[61]. Briefly, single-cell suspensions were stained with anti-CD11b-APC (1:200; clone M1/70, eBioscience) for 20 min and incubated with magnetic anti-APC MicroBeads according to the manufacturer's instructions (Miltenyi Biotec). CD11b$^+$ cells were isolated with LS columns (Miltenyi Biotec) according to the manufacturer's instructions. For the isolation of macrophages and neutrophils from tumours at the therapy-responsive phase, the enriched CD11b$^+$ fraction was stained with antibodies against Ly6G-FITC (1:200; clone 1A8, BD Biosciences), F4/80-PE (1:200; clone BM8, eBioscience) and Ly6C-ef450 (1:400; clone hk1.4, eBioscience). LIVE/DEAD fixable aqua dead cell stain (Thermo Fisher Scientific) was added 1:100 in PBS to exclude dead cells. CD11b$^+$F4/80$^+$ macrophages and F4/80$^-$Ly6G$^+$Ly6C^{low} neutrophils were isolated with the BD FACSARIA II sorter with DIVA software (BD Biosciences).

For the isolation of cell populations from end-stage tumours, we separated intratumoural CD11b$^+$ and CD11b$^-$ cells by magnetic cell sorting as described above. The CD11b$^-$ and CD11b$^+$ fractions were stained as described in Supplementary Table 1. CD11b$^+$F4/80$^+$ macrophages, CD11b$^+$F4/80$^-$Ly6G$^-$Ly6C$^+$ monocytes, CD11b$^+$F4/80$^-$Ly6G$^+$Ly6C^{low} neutrophils, CD11b$^-$CD45$^+$CD11c$^-$ lymphocytes and CD11b$^-$CD45$^-$CD31$^-$ tumour cells were isolated with BD FACSARIA FUSION sorter with DIVA software (BD Biosciences).

Adoptive transfer of monocytes

Front legs, hind legs and hips were collected from female mTmG mice and the bone marrow was flushed out. Bone marrow cells were incubated with Fc Block (1:50; CD16/CD32, BD Biosciences), stained with anti-Ly6G-APC (1:200; clone 1A8, BioLegend) and, consequently, negative selection for neutrophils was performed using magnetic columns (Miltenyi Biotec) as described previously[61]. The Ly6G$^-$ fraction was then stained with fluorochrome-conjugated antibodies (Supplementary

Table 1). After gating out Lineage$^+$ cells (CD3, CD8, CD4, NKp46 and Ter119) and Siglec F$^+$, Sca1$^+$ and cKIT$^+$ cells, tdTomato$^+$CD11b^{int}Ly6G$^-$Ly6C$^+$ monocytes were isolated with BD FACSARIA FUSION sorter with DIVA software (BD Biosciences). Between 1.5 and 2 × 10^6 tdTomato$^+$ monocytes were adoptively transfer into the tail vein of a tumour-bearing KEP mouse treated with control antibody or anti-CSF-1R. Antibody treatments started at a tumour size of 25 mm^2, and 1 d after the second antibody injection (1 week apart), monocytes were transferred. KEP mice were sacrificed 4 d later and tumours were isolated for flow cytometry analysis. Antibodies are listed in Supplementary Table 1.

CRISPR–Cas9-mediated gene disruption and colony-forming assay
IFNAR1 was knocked out (KO) from a cell line derived from a spontaneous KEP mammary tumour by transient transfection with a lentiCRISPRv2 (ref. [62]) containing IFNAR1-specific single guide RNA targeting exon 1 (sgRNA1: 5'-GCTCGCTGTCGTGGGCGCGG-3'). Twenty-four hours after transfection, cells were exposed to puromycin for 48 h. Cells were stained with IFNAR1-PE (1:200; clone MAR1-5A3, eBioscience) and IFNAR1-negative cells were sorted with BD FACSARIA FUSION sorter with DIVA software (BD Biosciences).

KEP and IFNAR1 KO KEP cells (250 cells per well) were seeded in triplicate in a 24-well plate, and the next day, cells were treated with an increasing concentration of recombinant IFN-α1 (BioLegend) for 7 d. On day 5, 4 μM or 8 μM cisplatin were added. At day 7, cells were washed, fixed in ice-cold methanol and incubated with 0.05% crystal violet. For quantification, crystal violet was dissolved in 10% acetic acid for 20 min and the absorbance was measured at 590 nm.

BMDMs
To generate BMDMs, bone marrow cells were harvested from the hind legs of wild-type mice and cultured for 7 days in RPMI medium containing 8% FCS, 100 IU ml^{-1} penicillin, 100 mg ml^{-1} streptomycin and 20 ng ml^{-1} recombinant M-CSF (Peprotech). After differentiation, BMDMs were harvested and seeded in a 24-well plate (400,000 BMDMs per well) and cultured overnight. The next morning, BMDMs were exposed to conditioned medium from a KEP cancer cell line in the presence of 8μg ml^{-1} of either control antibody or anti-CSF-1R for 24 h. Conditioned medium was obtained by culturing KEP cancer cells (80–90% confluency) for 24 h in RPMI containing 8% FCS, 100 IU ml^{-1} penicillin and 100 mg ml^{-1} streptomycin. The RNA of BMDMs was isolated with the Isolate II RNA Mini Kit (Bioline), and quantitative RT–PCR for *Ifna* was performed as described below.

RNA isolation and quantitative RT–PCR
RNA from sorted cells and tumours of KEP mice was isolated using TRIzol (Invitrogen). Samples were treated with DNase I (Invitrogen) followed by RNA cleanup with the Qiagen RNeasy Mini Kit according to the manufacturer's recommendation. Isolated RNA was quantified with Nanodrop (Thermo Scientific). Transformation of RNA into cDNA was performed with the Cloned AMV First-Strand cDNA Synthesis Kit (Invitrogen) using oligo(dT) primers. cDNA (20 ng per well) was analysed by SYBR green real-time PCR with 500 nM primers (Supplementary Table 2) using a

5

LightCycler 480 thermocycler (Roche). Samples were run in duplicate and were only further considered if the difference between the CT values of the duplo was less than one cycle. β-Actin was used as a reference gene.

Luminex cytokine array

Tumours and mammary glands were prepared with Bio-Rad cell lysis buffer, and the protein concentration of lysates was determined using the Pierce BCA Protein Assay Kit (Thermo Fischer Scientific) according to the manufacturer's recommendations. CSF-1 concentration in protein lysates was determined using the Bio-Plex Pro Cytokine 23-Plex Kits (Bio-Rad) and measured according to the manufacturer's instruction. Data acquisition and analysis were performed on a Bio-Plex 200 reader, using Bio-Plex Manager 6.0 software (Bio-Rad).

RNA-seq and data analysis

RNA isolation, library construction and deep sequencing

$CD11b^+F4/80^+$ and $CD11b^+F4/80^-Ly6G^+Ly6C^{low}$ immune cell populations were isolated as described above from KEP tumours treated with either control antibody, anti-CSF-1R, cisplatin + control antibody or cisplatin + anti-CSF-1R at the therapy-responsive phase (tumour size ± 100 mm²). Some of the biological replicates consisted of pools of cells from two to six different mice. Total RNA was extracted using the RNeasy Mini and Microkits (Qiagen). According to the Ovation RNA-seq system V2 and Encore Rapid library systems protocols (NuGen), 10 ng RNA was converted into cDNA libraries, subsequently sequenced on a HiSeq 1500 system and demultiplexed using CASAVA v1.8 (Illumina).

Preprocessing of sequenced data

Using default parameters, all reads were aligned against the murine mm10 reference genome by TopHat2 v2.0.11 (ref. [63]). The data were imported into Partek Genomics Suite v6.6 (PGS), and the gene and transcript information was deducted before conducting normalization utilizing statistical software R (v3.3.1) and the DESeq2 package (https://doi.org/10.1101/002832). Normalized read counts were floored to a value of at least one thereafter and the data set was trimmed by defining a gene as expressed if the maximum value over all group means was higher than ten.

Identification of differentially expressed genes

Using PGS, a two-way analysis of variance (ANOVA) was performed to compute the top variable genes (treatment versus control) within the data set, as well as differentially expressed genes present in cisplatin + anti-CSF-1R neutrophils (versus cisplatin + control antibody neutrophils). Genes were defined to be differentially expressed when having a fold change of ≥1.5 and an unadjusted $P ≤ 0.05$. Based on the ANOVA model, hierarchical clustering was performed on the top 400 variable genes within the data set (neutrophils and macrophages, cisplatin + anti-CSF-1R versus cisplatin + control antibody) using default settings in PGS.

Gene Ontology enrichment analysis, Gene Ontology network visualization, Ingenuity pathway analysis and GSEA
To link transcriptome information to previous knowledge, we applied Gene Ontology enrichment analysis on the 100 most upregulated and 100 most downregulated genes (fold change ≥ 1.5, unadjusted $P \leq 0.05$) extracted from neutrophils exposed to cisplatin + anti-CSF-1R treatment (versus cisplatin + control antibody-exposed neutrophils). Subsequently, the data were visualized using BiNGO[64], EnrichmentMap[65] and Word Clouding[66] plug-ins in Cytoscape. In addition, all differentially expressed genes found in neutrophils were analysed with Ingenuity pathway analysis (Qiagen).

GSEA was performed utilizing the BubbleGUM GSEA tool[67] to find enriched pathways in macrophages from cisplatin + anti-CSF-1R-treated tumours (versus cisplatin + control antibody macrophages). Pathways interrogated were derived from the reactome gene sets, and all pathways demonstrating a significant enrichment (false discovery rate (FDR) ≤ 0.25) in one condition were shown. Specifically addressing enrichment of EGR2 target genes in neutrophils from anti-CSF-1R-treated tumours versus neutrophils from control antibody-treated tumours, GSEA was employed on transcription factor target gene sets using the GSEA tool previously published[68]. The reactome and transcription factor target gene sets were obtained via the online available Molecular Signatures Database (MSigDB) of the Broad Institute (http://software.broadinstitute.org/gsea/msigdb/index.jsp).
No custom codes were used in the manuscript.

Evaluation of expression of ISGs in patient biopsies
The selection of type I ISGs was based on the RNA-seq results from our KEP mouse model upon cisplatin + anti-CSF-1R. The genes belong to the biological processes listed in Supplementary Table 3. We assessed the effect of anti-CSF-1R on these selected genes in human tumours by analysing RNA-seq data of paired baseline and on-treatment tumour biopsies of patients enrolled in a clinical phase I trial with emactuzumab (RG7155), a humanized anti-human CSF-1R monoclonal antibody. Biopsies were taken from a multicentre, open-label study (ClinicalTrials.gov identifier NCT01494688). Patients received emactuzumab every 2 weeks as intravenous infusion. Tumour biopsies of 31 patients with a broad range of different solid malignancies treated with either emactuzumab alone or in combination with paclitaxel (with an overrepresentation of breast cancer ($n = 13$) and ovarian cancer ($n = 7$) samples) were collected. The study was conducted in accordance with the Declaration of Helsinki, current International Conference on Harmonisation of Technical Requirements for Registration of Pharmaceuticals for Human Use guidelines and all applicable regulatory and ethical requirements. The study is compliant with all relevant ethical regulations regarding research involving human participants. All patients provided written informed consent before study-related procedures were performed. RNA extraction, RNA-seq and data analysis were performed as previously described[69].

5

Statistics and reproducibility
Information on study design, sample size, number of biological replicates, number of independent experiments and statistical analysis is reported in the main text and figure legends. The survival curves of cisplatin + control antibody (or cisplatin only)-treated, cisplatin + anti-CSF-1R-treated and cisplatin + anti-CSF-1R + anti-Ly6G-treated mice were repeated and confirmed in a separate animal facility (Figs. 1f and 6d–f); other in vivo interventions were performed once. In vitro experiments were repeated independently with similar results. Statistical analyses were performed using GraphPad Prism 7 and 8 (GraphPad Software Inc.). The two-tailed Mann–Whitney test was used for immunohistochemistry and flow cytometry analysis. Two-way ANOVA with Tukey's multiple comparison test was used for the quantification of crystal violet absorbance. Two-tailed log-rank tests were used for Kaplan–Meier survival curves. Fisher's exact test (two-sided) was used for metastasis analysis. $P < 0.05$ was considered statistically significant.

Reporting Summary
Further information on research design is available in the Nature Research Reporting Summary linked to this article.

Data availability

The RNA-seq data derived from mouse samples that support the findings of this study have been deposited in the Gene Expression Omnibus (GEO) repository under accession number GSE101881. Source data for Figs. 1a,d–i, 2, 3c–h, 4, 5 and 6 and Supplementary Figs. 1a,b,e,f,h,i, 2, 3e–h, 5a–c,f–i and 6a–f,i–n have been provided as Supplementary Table 4. All other data supporting the findings of this study are available from the corresponding author on reasonable request.

Additional information

Publisher's note: Springer Nature remains neutral with regard to jurisdictional claims in published maps and institutional affiliations.

Acknowledgements

Contributions

C.S., M.C., C.H.R., J.J. and K.E.d.V. conceived the ideas and designed the experiments. C.S., M.C., C.-S.H., S.B.C., K. Kersten, A.v.W., K.V., K. Kos and K.E.d.V. performed the experiments and analysed the data. C.H.R. provided the anti-CSF-1R antibody and control antibody. S.T., T.U. and J.L.S. prepared the samples and conducted the RNA-seq and bioinformatics analyses on murine cells. J.-Y.S. performed the metastasis scoring. C.-H.O., D.R. and P.A.C. were involved in the collection of patient samples and bioinformatic analysis of the human data. C.S. and K.E.d.V. wrote the paper.

Competing interests

C.H.R., C.-H.O. and D.R. are employees of F. Hoffman La Roche. C.H.R. is an inventor of granted and pending patent applications relating to emactuzumab and a stockholder in F. Hoffman La Roche. F. Hoffman La Roche provided financial research support for the experiments with anti-CSF-1R. P.A.C. received funding from Roche for the described clinical trial and other Roche-sponsored studies.

5

References

1. Coffelt, S. B. & de Visser, K. E. Immune-mediated mechanisms influencing the efficacy of anticancer therapies. *Trends Immunol.* **36**, 198–216 (2015).
2. Galluzzi, L., Buque, A., Kepp, O., Zitvogel, L. & Kroemer, G. Immunogenic cell death in cancer and infectious disease. *Nat. Rev. Immunol.* **17**, 97–111 (2017).
3. Ciampricotti, M., Hau, C. S., Doornebal, C. W., Jonkers, J. & de Visser, K. E. Chemotherapy response of spontaneous mammary tumors is independent of the adaptive immune system. *Nat. Med.* **18**, 344–346 (2012).
4. DeNardo, D. G. et al. Leukocyte complexity predicts breast cancer survival and functionally regulates response to chemotherapy. *Cancer Discov.* **1**, 54–67 (2011).
5. Ruffell, B. et al. Macrophage IL-10 blocks CD8^{+} T cell-dependent responses to chemotherapy by suppressing IL-12 expression in intratumoral dendritic cells. *Cancer Cell* **26**, 623–637 (2014).
6. Campbell, M. J. et al. The prognostic implications of macrophages expressing proliferating cell nuclear antigen in breast cancer depend on immune context. *PLoS One* **8**, e79114 (2013).
7. Chua, W., Charles, K. A., Baracos, V. E. & Clarke, S. J. Neutrophil/lymphocyte ratio predicts chemotherapy outcomes in patients with advanced colorectal cancer. *Br. J. Cancer* **104**, 1288–1295 (2011).
8. Kishi, Y. et al. Blood neutrophil-to-lymphocyte ratio predicts survival in patients with colorectal liver metastases treated with systemic chemotherapy. *Ann. Surg. Oncol.* **16**, 614–622 (2009).
9. Miao, Y., Yan, Q., Li, S., Li, B. & Feng, Y. Neutrophil to lymphocyte ratio and platelet to lymphocyte ratio are predictive of chemotherapeutic response and prognosis in epithelial ovarian cancer patients treated with platinum-based chemotherapy. *Cancer Biomark.* **17**, 33–40 (2016).
10. Pistelli, M. et al. Pre-treatment neutrophil to lymphocyte ratio may be a useful tool in predicting survival in early triple negative breast cancer patients. *BMC Cancer* **15**, 195 (2015).
11. Paulus, P., Stanley, E. R., Schafer, R., Abraham, D. & Aharinejad, S. Colony-stimulating factor-1 antibody reverses chemoresistance in human MCF-7 breast cancer xenografts. *Cancer Res.* **66**, 4349–4356 (2006).
12. Shree, T. et al. Macrophages and cathepsin proteases blunt chemotherapeutic response in breast cancer. *Genes Dev.* **25**, 2465–2479 (2011).
13. Mitchem, J. B. et al. Targeting tumor-infiltrating macrophages decreases tumor-initiating cells, relieves immunosuppression, and improves chemotherapeutic responses. *Cancer Res.* **73**, 1128–1141 (2013).
14. Di Mitri, D. et al. Tumour-infiltrating Gr-1^{+} myeloid cells antagonize senescence in cancer. *Nature* **515**, 134–137 (2014).
15. Houthuijzen, J. M. et al. Lysophospholipids secreted by splenic macrophages induce chemotherapy resistance via interference with the DNA damage response. *Nat. Commun.* **5**, 5275 (2014).
16. Acharyya, S. et al. A CXCL1 paracrine network links cancer chemoresistance and metastasis. *Cell* **150**, 165–178 (2012).
17. Olson, O. C., Kim, H., Quail, D. F., Foley, E. A. & Joyce, J. A. Tumor-associated macrophages suppress the cytotoxic activity of antimitotic agents. *Cell Rep.* **19**, 101–113 (2017).
18. Weizman, N. et al. Macrophages mediate gemcitabine resistance of pancreatic adenocarcinoma by upregulating cytidine deaminase. *Oncogene* **33**, 3812–3819 (2014).
19. Nakasone, E. S. et al. Imaging tumor–stroma interactions during chemotherapy reveals contributions of the microenvironment to resistance. *Cancer Cell* **21**, 488–503 (2012).
20. Nywening, T. M. et al. Targeting both tumour-associated CXCR2^{+} neutrophils and CCR2^{+} macrophages disrupts myeloid recruitment and improves chemotherapeutic responses in pancreatic ductal adenocarcinoma. *Gut* **67**, 1112–1123 (2018).
21. Ries, C. H. et al. Targeting tumor-associated macrophages with anti-CSF-1R antibody reveals a strategy for cancer therapy. *Cancer Cell* **25**, 846–859 (2014).
22. Quail, D. F. & Joyce, J. A. Molecular pathways: deciphering mechanisms of resistance to

macrophage-targeted therapies. *Clin. Cancer Res.* **23**, 876–884 (2017).

23. Crusz, S. M. & Balkwill, F. R. Inflammation and cancer: advances and new agents. *Nat. Rev. Clin. Oncol.* **12**, 584–596 (2015).

24. Derksen, P. W. et al. Somatic inactivation of E-cadherin and p53 in mice leads to metastatic lobular mammary carcinoma through induction of anoikis resistance and angiogenesis. *Cancer Cell* **10**, 437–449 (2006).

25. Hume, D. A. & MacDonald, K. P. Therapeutic applications of macrophage colony-stimulating factor-1 (CSF-1) and antagonists of CSF-1 receptor (CSF-1R) signaling. *Blood* **119**, 1810–1820 (2012).

26. Franklin, R. A. et al. The cellular and molecular origin of tumor-associated macrophages. *Science* **344**, 921–925 (2014).

27. Doornebal, C. W. et al. A preclinical mouse model of invasive lobular breast cancer metastasis. *Cancer Res.* **73**, 353–363 (2013).

28. Noy, R. & Pollard, J. W. Tumor-associated macrophages: from mechanisms to therapy. *Immunity* **41**, 49–61 (2014).

29. Bradley, E. W., Ruan, M. M. & Oursler, M. J. Novel pro-survival functions of the Kruppel-like transcription factor Egr2 in promotion of macrophage colony-stimulating factor-mediated osteoclast survival downstream of the MEK/ERK pathway. *J. Biol. Chem.* **283**, 8055–8064 (2008).

30. Gomez-Roca, C. A. et al. Phase I study of RG7155, a novel anti-CSF1R antibody, in patients with advanced/metastatic solid tumors. *J. Clin. Oncol.* **33**, 3005 (2015).

31. Zitvogel, L., Galluzzi, L., Kepp, O., Smyth, M. J. & Kroemer, G. Type I interferons in anticancer immunity. *Nat. Rev. Immunol.* **15**, 405–414 (2015).

32. Vacchelli, E. et al. Autocrine signaling of type 1 interferons in successful anticancer chemotherapy. *Oncoimmunology* **4**, e988042 (2015).

33. Parker, B. S., Rautela, J. & Hertzog, P. J. Antitumour actions of interferons: implications for cancer therapy. *Nat. Rev. Cancer* **16**, 131–144 (2016).

34. Snell, L. M., McGaha, T. L. & Brooks, D. G. Type I interferon in chronic virus infection and cancer. *Trends Immunol.* **38**, 542–557 (2017).

35. Fuertes, M. B. et al. Host type I IFN signals are required for antitumor CD8+ T cell responses through CD8α+ dendritic cells. *J. Exp. Med.* **208**, 2005–2016 (2011).

36. Coffelt, S. B. et al. IL-17-producing γδ T cells and neutrophils conspire to promote breast cancer metastasis. *Nature* **522**, 345–348 (2015).

37. Sistigu, A. et al. Cancer cell-autonomous contribution of type I interferon signaling to the efficacy of chemotherapy. *Nat. Med.* **20**, 1301–1309 (2014).

38. Burnette, B. C. et al. The efficacy of radiotherapy relies upon induction of type I interferon-dependent innate and adaptive immunity. *Cancer Res.* **71**, 2488–2496 (2011).

39. Deng, L. et al. STING-dependent cytosolic DNA sensing promotes radiation-induced type I interferon-dependent antitumor immunity in immunogenic tumors. *Immunity* **41**, 843–852 (2014).

40. Bidwell, B. N. et al. Silencing of Irf7 pathways in breast cancer cells promotes bone metastasis through immune escape. *Nat. Med.* **18**, 1224–1231 (2012).

41. Callari, M. et al. Subtype-dependent prognostic relevance of an interferon-induced pathway metagene in node-negative breast cancer. *Mol. Oncol.* **8**, 1278–1289 (2014).

42. Snijders, A. M. et al. An interferon signature identified by RNA-sequencing of mammary tissues varies across the estrous cycle and is predictive of metastasis-free survival. *Oncotarget* **5**, 4011–4025 (2014).

43. Schiavoni, G. et al. Cyclophosphamide synergizes with type I interferons through systemic dendritic cell reactivation and induction of immunogenic tumor apoptosis. *Cancer Res.* **71**, 768–778 (2011).

44. Weichselbaum, R. R. et al. An interferon-related gene signature for DNA damage resistance is a predictive marker for chemotherapy and radiation for breast cancer. *Proc. Natl Acad. Sci. USA* **105**, 18490–18495 (2008).

5

45. Critchley-Thorne, R. J. et al. Impaired interferon signaling is a common immune defect in human cancer. *Proc. Natl Acad. Sci. USA* **106**, 9010–9015 (2009).

46. Pyonteck, S. M. et al. CSF-1R inhibition alters macrophage polarization and blocks glioma progression. *Nat. Med.* **19**, 1264–1272 (2013).

47. Quail, D. F. et al. The tumor microenvironment underlies acquired resistance to CSF-1R inhibition in gliomas. *Science* **352**, aad3018 (2016).

48. Yan, D. et al. Inhibition of colony stimulating factor-1 receptor abrogates microenvironment-mediated therapeutic resistance in gliomas. *Oncogene* **36**, 6049–6058 (2017).

49. Zhu, Y. et al. CSF1/CSF1R blockade reprograms tumor-infiltrating macrophages and improves response to T-cell checkpoint immunotherapy in pancreatic cancer models. *Cancer Res.* **74**, 5057–5069 (2014).

50. Coffelt, S. B., Wellenstein, M. D. & de Visser, K. E. Neutrophils in cancer: neutral no more. *Nat. Rev. Cancer* **16**, 431–446 (2016).

51. Pylaeva, E., Lang, S. & Jablonska, J. The essential role of type I interferons in differentiation and activation of tumor-associated neutrophils. *Front. Immunol.* **7**, 629 (2016).

52. Berry, M. P. et al. An interferon-inducible neutrophil-driven blood transcriptional signature in human tuberculosis. *Nature* **466**, 973–977 (2010).

53. Rocha, B. C. et al. Type I interferon transcriptional signature in neutrophils and low-density granulocytes are associated with tissue damage in malaria. *Cell Rep.* **13**, 2829–2841 (2015).

54. Teijaro, J. R. et al. Persistent LCMV infection is controlled by blockade of type I interferon signaling. *Science* **340**, 207–211 (2013).

55. Cunningham, C. R. et al. Type I and type II interferon coordinately regulate suppressive dendritic cell fate and function during viral persistence. *PLoS Pathog.* **12**, e1005356 (2016).

56. Corrales, L. et al. Direct activation of STING in the tumor microenvironment leads to potent and systemic tumor regression and immunity. *Cell Rep.* **11**, 1018–1030 (2015).

57. Muzumdar, M. D., Tasic, B., Miyamichi, K., Li, L. & Luo, L. A global double-fluorescent Cre reporter mouse. *Genesis* **45**, 593–605 (2007).

58. Michaut, M. et al. Integration of genomic, transcriptomic and proteomic data identifies two biologically distinct subtypes of invasive lobular breast cancer. *Sci. Rep.* **6**, 18517 (2016).

59. Schouten, P. C. et al. Robust BRCA1-like classification of copy number profiles of samples repeated across different datasets and platforms. *Mol. Oncol.* **9**, 1274–1286 (2015).

60. Wang, F. et al. RNAscope: a novel in situ RNA analysis platform for formalin-fixed, paraffin-embedded tissues. *J. Mol. Diagn.* **14**, 22–29 (2012).

61. Salvagno, C. & de Visser, K. E. Purification of immune cell populations from freshly isolated murine tumors and organs by consecutive magnetic cell sorting and multi-parameter flow cytometry-based sorting. *Methods Mol. Biol.* **1458**, 125–135 (2016).

62. Sanjana, N. E., Shalem, O. & Zhang, F. Improved vectors and genome-wide libraries for CRISPR screening. *Nat. Methods* **11**, 783–784 (2014).

63. Kim, D. et al. TopHat2: accurate alignment of transcriptomes in the presence of insertions, deletions and gene fusions. *Genome Biol.* **14**, R36 (2013).

64. Maere, S., Heymans, K. & Kuiper, M. BiNGO: a Cytoscape plugin to assess overrepresentation of gene ontology categories in biological networks. *Bioinformatics* **21**, 3448–3449 (2005).

65. Merico, D., Isserlin, R., Stueker, O., Emili, A. & Bader, G. D. Enrichment map: a network-based method for gene-set enrichment visualization and interpretation. *PLoS One* **5**, e13984 (2010).

66. Oesper, L., Merico, D., Isserlin, R. & Bader, G. D. WordCloud: a Cytoscape plugin to create a visual semantic summary of networks. *Source Code Biol. Med.* **6**, 7 (2011).

67. Spinelli, L., Carpentier, S., Montanana Sanchis, F., Dalod, M. & Vu Manh, T. P. BubbleGUM: automatic extraction of phenotype molecular signatures and comprehensive visualization of multiple gene set enrichment analyses. *BMC Genomics* **16**, 814 (2015).

68. Subramanian, A. et al. Gene set enrichment analysis: a knowledge-based approach for interpreting genome-wide expression profiles. *Proc. Natl Acad. Sci. USA* **102**, 15545–15550 (2005).

69. Pradel, L. P. et al. Macrophage susceptibility to emactuzumab (RG7155) treatment. *Mol. Cancer Ther.* **15**, 3077–3086 (2016).

5
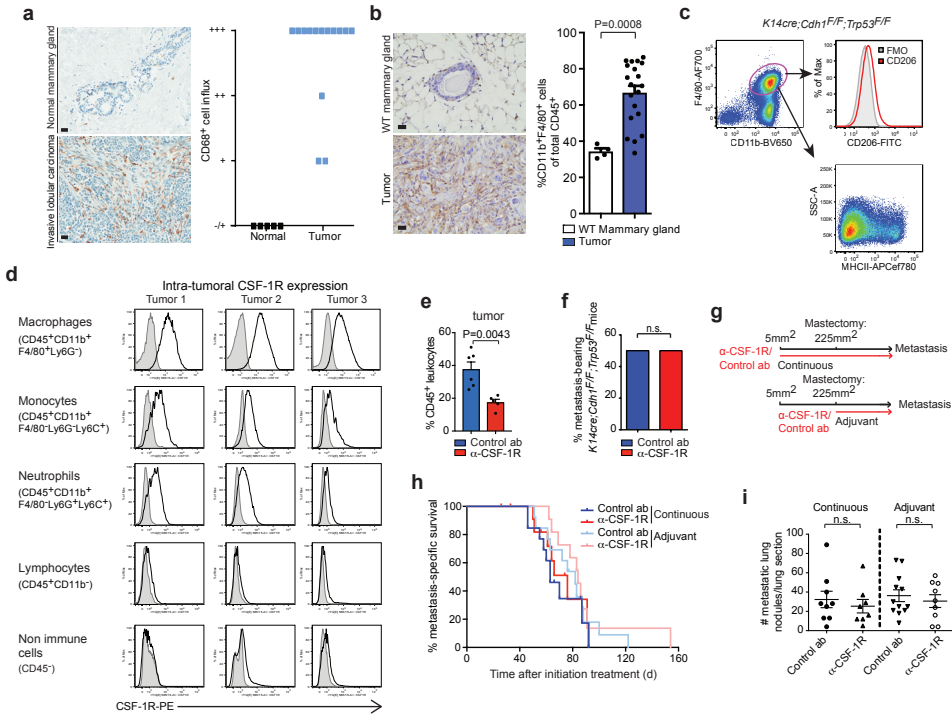
Supplementary Fig. 1 | CSF-1R blockade does not influence spontaneous metastasis formation. **(a)** Presence of CD68⁺ macrophages in untreated human invasive lobular carcinomas and in adjacent normal breast tissue. Influx of CD68⁺ macrophages was scored based on immunohistochemistry (normal breast tissue, n=5 patients; invasive lobular carcinomas, n=14 patients). Representative images are shown. Scale bar=25µm. **(b)** Representative IHC staining of F4/80⁺ macrophages in a mammary tumor of a KEP mouse and in a normal mammary gland of an age-matched WT mouse. Scale bar=20µm. Percentage of CD11b⁺F4/80⁺ macrophages gated on CD45⁺ cells in KEP mammary tumors (n=20 animals) and in normal mammary glands of age-matched WT mice (n=4 animals). **(c)** Representative flow cytometry histogram and plot showing CD206 and MHCII expression, respectively, on F4/80⁺ macrophages in a KEP mammary tumor. Data are representative of 5 independent KEP mammary tumors. **(d)** Flow cytometry histograms showing CSF-1R expression levels (white) and Fluorescence minus one (FMO) control (grey) in 3 independent KEP mammary tumors. **(e)** Proportion of CD45⁺ immune cells of total live cells in tumors of time point-sacrificed KEP mice treated with control ab (n=6 animals) or anti-CSF-1R (n=5 animals) as determined by flow cytometry. **(f)** Organs collected from KEP mice bearing end-stage mammary tumors treated with control ab (n=20 animals) or anti-CSF-1R (n=22 animals) were microscopically analyzed for the presence of metastases. Percentage of tumor-bearing KEP mice with metastases is displayed. p=0.1 by Fisher's exact test (Two-sided). **(g)** Schematic overview of continuous and adjuvant antibody treatment in the KEP-based spontaneous metastasis model as described in Methods. **(h)** Kaplan-Meier metastasis-specific survival curves of recipient mice orthotopically transplanted with tumor fragments from KEP mice and treated either continuously (control ab n=13 animals, anti-CSF-1R n=14 animals) or in an adjuvant setting (control ab n=13 animals, anti-CSF-1R n=11 animals). An event is defined as an animal that was sacrificed because of clinical signs of metastatic disease. **(i)** Quantification of the number of spontaneous pulmonary metastases in mice treated either continuously (control ab n=9 animals; anti-CSF-1R n=8 animals) or in an adjuvant setting (Control ab n=12 animals; anti-CSF-1R n=9 animals). Data presented in **b, e** and **i** are mean ± SEM and statistical analysis was performed using two-tailed Mann–Whitney test.
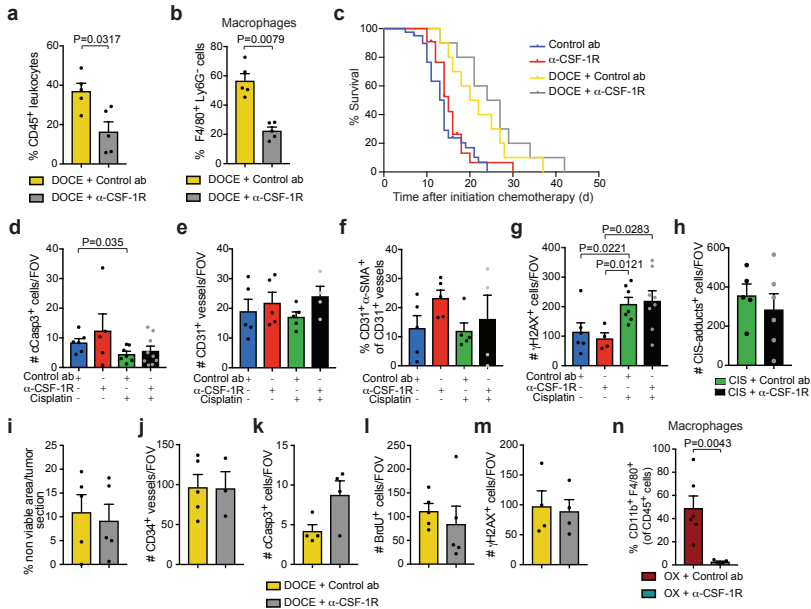
Supplementary Fig. 2 | CSF-1R blockade synergizes with platinum-based chemotherapy drugs, and not with docetaxel. (a-b) Proportion of CD45^{+} immune cells gated on live cells **(a)** and F4/80^{+}Ly6G^{-} macrophages gated on CD11b^{+} cells **(b)** determined by flow cytometry in tumors of time point-sacrificed KEP mice treated as indicated (n=5 animals/group). **(c)** Kaplan Meier tumor-specific survival curves of KEP mice treated with control ab, anti-CSF-1R (same groups as Fig. 1f), docetaxel/control ab (n=10 animals) or docetaxel/anti-CSF-1R (n=10 animals). Docetaxel/control ab versus Control ab, p=0.0021; Docetaxel/control ab versus docetaxel/anti-CSF-1R, p=0.329 (two-tailed log-rank test). **(d)** Quantification of cleaved caspase 3^{+} cells in viable areas of mammary tumors of time point-sacrificed KEP mice treated with control ab (n=6 animals), anti-CSF-1R (n=5 animals), cisplatin/control ab (n=7 animals) and cisplatin/anti-CSF-1R (n=9 animals) as determined by IHC. **(e)** Quantification of CD31^{+} vessels in viable areas of mammary tumors of time point-sacrificed KEP mice treated with control ab (n=5 animals), anti-CSF-1R (n=5 animals), cisplatin/control ab (n=5 animals) and cisplatin/anti-CSF-1R (n=4 animals) as determined by immunofluorescence. Values represent average number of positive cells per FOV quantified by counting six fields per tumor. **(f)** Percentage of vessels covered by alpha-SMA[+] pericytes in viable areas of mammary tumors as determined by immunofluorescence. Same mice as **e**. Percentage was determined by counting alpha-SMA^{+}CD31^{+} cells and total CD31^{+} cells in six high-power microscopic fields per tumor. **(g-h)** Quantification of γH2AX^{+} cells **(g)** and cisplatin adducts^{+} cells **(h)** in viable areas of mammary tumors of time point-sacrificed KEP mice treated as indicated (γH2AX: control ab n=6 animals, anti-CSF-1R n=4 animals, cisplatin/control ab n=7 animals, cisplatin/anti-CSF-1R n=8 animals; CIS-adducts: cisplatin/control ab n=5 animals, cisplatin/anti-CSF-1R n=6 animals). **(i)** Percentage of non-viable area per tumor section of time point-sacrificed KEP mice quantified by digital area analysis of H&E stained sections (n=5 animals/group). **(j-m)** Quantification of CD34^{+} cells **(j)**, cleaved caspase 3^{+} cells **(k)**, BrdU^{+} cells **(l)**, γH2AX^{+} cells **(m)** in viable areas of mammary tumors of time point-sacrificed KEP mice treated as indicated (CD34: docetaxel/control ab n=5 animals, docetaxel/anti-CSF-1R n=3 animals; cCasp3: n=4 animals/group; BrdU: n=5 animals/group; γH2AX: n=4 animals/group). **(n)** Proportion of CD11b^{+}F4/80^{+} macrophages gated on CD45^{+} cells as determined by flow cytometry in tumors of end-stage KEP mice treated as indicated (oxaliplatin/Control ab treatment n=6 animals; oxaliplatin/anti-CSF-1R treatment n=5 animals). Data presented in **d, g-h, j-m** show average number of positive cells per field of view (FOV) quantified by counting five high-power microscopic fields per tumor. Data presented in **a-b** and **d-n** are mean values ± SEM and statistical analysis was performed using two-tailed Mann–Whitney test. DOCE, docetaxel, CIS, cisplatin, OX, oxaliplatin.

5
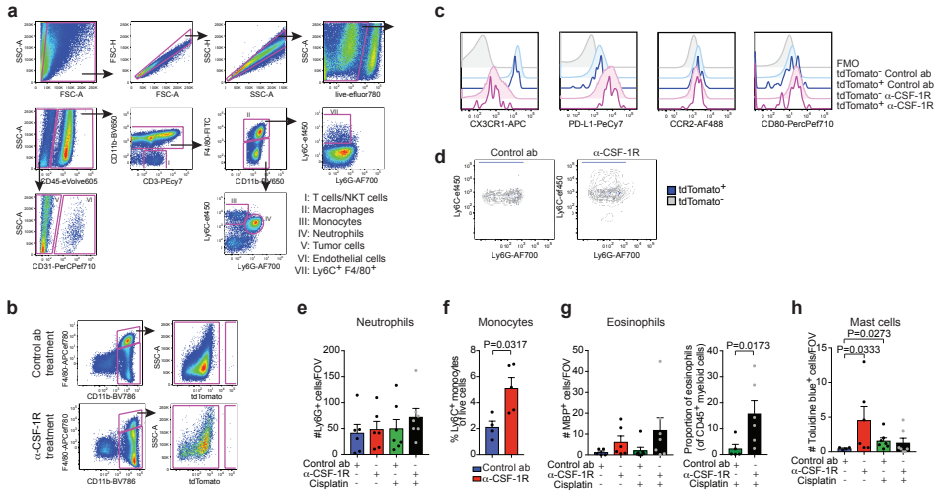
Supplementary Fig. 3 | Impact of CSF-1R inhibition on the intratumoral presence of diverse myeloid immune cell types. (a) Representative dot plots of a KEP mammary tumor illustrating the gating strategy for the identification of cell populations. Antibody panel used: "tumor panel I" (see supplementary Table 1). Arrows indicate directionality of sub-gates. **(b-d)** tdTomato^{+} (Lineage^{-} SiglecF[-]cKIT^{-}CD11b^{int}Ly6G^{-}Ly6C^{+}) monocytes were isolated from the bone marrow of mTmG mice and adoptively transferred into tumor-bearing KEP mice that had previously received either control ab or anti-CSF-1R. 4 days after the monocyte transfer, the presence and phenotype of tdTomato^{+} cells in tumors were analyzed. **(b)** Gating strategy showing intratumoral tdTomato^{+} cells that express F4/80 in control ab- or anti-CSF-1R-treated recipient KEP mice. **(c)** Representative flow cytometry histograms showing CX3CR1, PD-L1, CCR2 and CD80 expression in tdTomato[+] and tdTomato[-] macrophages in KEP tumors. **(d)** Overlay of representative dot plots showing Ly6C expression in tdTomato[+] and tdTomato[-] macrophages in control ab- and anti-CSF-1R-treated KEP mice. Data presented in **b-d** are representative of 2 (control ab treatment) and 3 (anti-CSF-1R treatment) independent experiments. **(e)** Quantification of Ly6G^{+} neutrophils in viable areas of mammary tumors of time point-sacrificed KEP mice treated with control ab (n=6 animals), anti-CSF-1R (n=6 animals), cisplatin/control ab (n=7 animals) or cisplatin/anti-CSF-1R (n=7 animals). **(f)** Proportion of Ly6C^{+}Ly6G^{-} monocytes determined by flow cytometry in KEP mammary tumors treated with control ab (n=4 animals) or anti-CSF-1R (n=5 animals). **(g)** Quantification of Major Basic Protein (MBP)[+] cells in viable areas of mammary tumors of time point-sacrificed KEP mice as determined by IHC (control ab n=5 animals, anti-CSF-1R n=6 animals, cisplatin/control ab n=7 animals, cisplatin/anti-CSF-1R n=7 animals) and proportion of Siglec F^{+} eosinophils gated on intratumoral CD45^{+} cells of time point-sacrificed KEP mice as determined by flow cytometry (cisplatin/control ab n=5 animals, cisplatin/anti-CSF-1R n=6 animals). **(h)** Quantification of Toluidine Blue^{+} mast cells in viable areas of mammary tumors of time point-sacrificed KEP mice (control ab n=4 animals, anti-CSF-1R n=6 animals, cisplatin/control ab n=7 animals, cisplatin/anti-CSF-1R n=7 animals) as determined by histochemistry. Values in **e**, **g** and **h** represent average number of positive cells per field of view (FOV) quantified by counting five high-power microscopic fields per tumor. Data presented in **e-h** are mean values ± SEM. Statistical analysis was performed using two-tailed Mann–Whitney test.
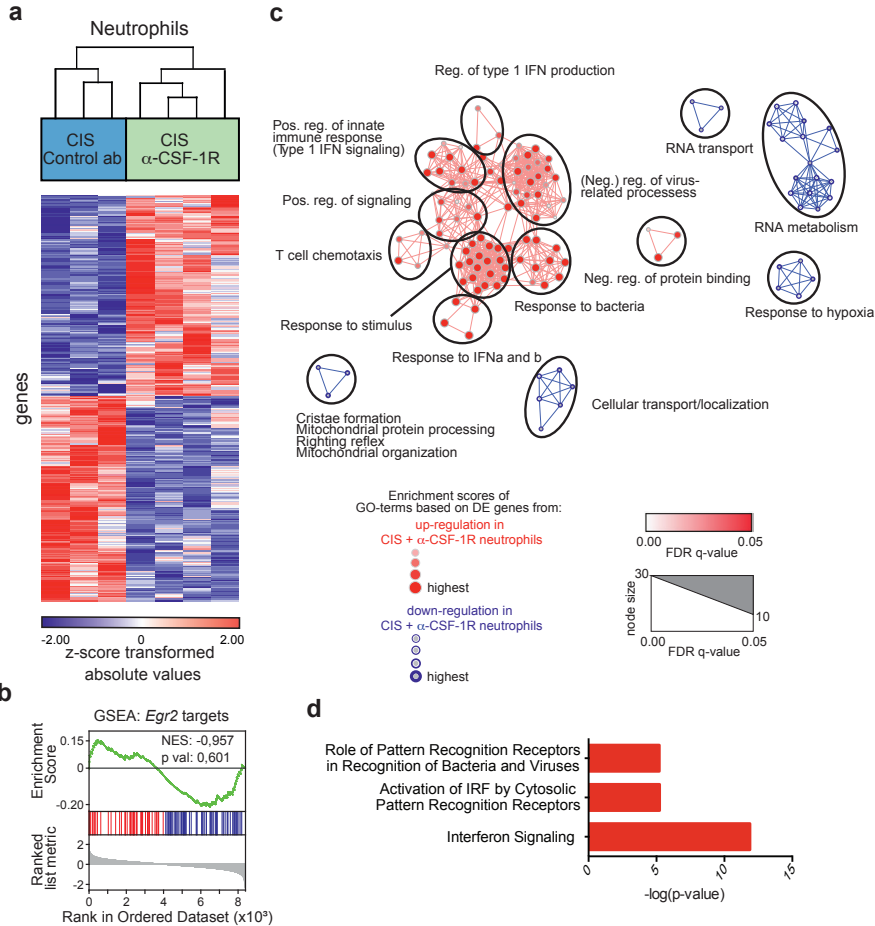
Supplementary Fig. 4 | Intratumoral neutrophils show elevated expression levels of type I IFN-stimulated genes upon CSF-1R blockade. (a) Hierarchical clustering of the top 400 variable genes between neutrophils isolated from tumors of KEP mice treated with cisplatin/control ab (n=3 biologically independent samples) and cisplatin/anti-CSF-1R (n=4 biologically independent samples). Mice were sacrificed one day after second cisplatin injection. FC: ≥ 1,5; unadjusted p-value: ≤ 0,05. Statistical analysis was performed using two-way ANOVA. **(b)** Gene set enrichment analysis (GSEA) of Egr2 target genes obtained from RNA-Seq data in tumor-infiltrating neutrophils of anti-CSF-1R-treated KEP mice compared to control ab-treated KEP mice (n=4 animals/group). Enrichment scores were calculated using a weighted Kolmogorov–Smirnov-like statistic. **(c)** Network visualization of GOEA of the top 100 up-regulated and top 100 down-regulated genes (cisplatin/anti-CSF-1R vs. cisplatin/control ab neutrophils; FC: 1,5, unadjusted p-value: ≤ 0.05) using BiNGO and EnrichmentMap. Red and blue nodes represent the positively and negatively enriched GO-terms, respectively. Node size represents corresponding enrichment p-values (FDR corrected p-value: ≤ 0.05). The genes used as input for the BiNGO analysis are derived from the 2-way ANOVA model. The enrichment score was calculated with a hypergeometric statistical test, multiple testing correction was performed with the Benjamin & Hochberg FDR correction. **(d)** Top three canonical pathways identified using ingenuity pathway analysis (IPA) enriched in neutrophils isolated from cisplatin/anti-CSF-1R-treated tumors (n=4 biologically independent samples) compared to neutrophils from cisplatin/control ab-treated tumors (n=3 biologically independent samples). Statistical analysis was performed with standard IPA software statistics.
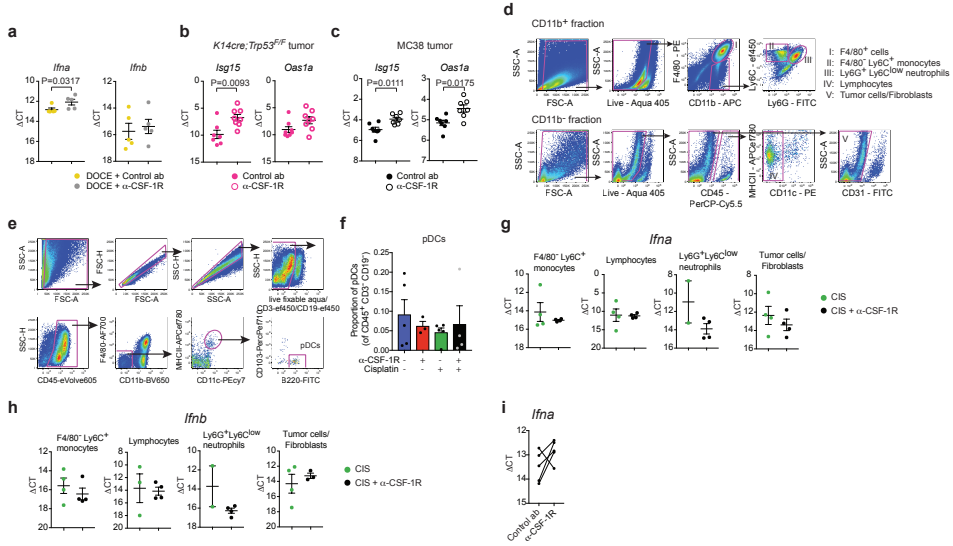
Supplementary Fig. 5 | CSF-1R blockade increases intratumoral *Ifna* expression. (a) Transcripts of *Ifna* and *Ifnb* in KEP mammary tumors were determined by qPCR and normalized to β-actin (n=5 animals/group). Mice were analyzed one day after the second docetaxel injection. Graphs show the mean ± SEM in ΔCt values. **(b-c)** Transcripts of *Isg15* and *Oas1a* in orthotopically transplanted *K14cre;Trp53^F/F^* (KP) tumors (*Isg15*: control ab n=7 animals, anti-CSF-1R n=8 animals; *Oas1a*: n=8 animals/group) **(b)** and subcutaneous MC38 tumors (n=8 animals/group) **(c)** treated as indicated were determined by qPCR and normalized to β-actin. Mice were analysed at a tumor size of 100mm² (KP) or after 12 days from the start of the treatment (MC38). Graphs show the mean ± SEM in ΔCt values. **(d)** Representative dot plots of a KEP tumor illustrating the gating strategy for cell sorting by flow cytometry. After cell separation based on CD11b expression by magnetic columns, the CD11b⁺ and CD11b⁻ fractions were stained as described in Methods followed by flow cytometry-based sorting of intratumoral cell populations. **(e)** Representative dot plots of a KEP tumor illustrating the gating strategy for the identification of pDCs. Antibody panel "tumor panel II" was used. Arrows indicate directionality of sub-gates. **(f)** Proportion of plasmacytoid dendritic cells (pDCs) in mammary tumors of end-stage KEP mice as determined by flow cytometry (control ab n=5 animals, anti-CSF-1R n=3 animals, cisplatin/control ab n=5 animals, cisplatin/anti-CSF-1R n=4 animals). **(g-h)** Transcripts of *Ifna* and *Ifnb* in CD11b⁺F4/80⁻Ly6G⁻Ly6C⁺ monocytes (*Ifna* and *Ifnb*: n=4 animals/group), CD45⁺CD11b⁻CD11c⁻ lymphocytes (*Ifna*: n=4 animals/group; *Ifnb*: cisplatin/control ab n=3 animals, cisplatin/anti-CSF-1R n=4 animals), CD11b⁺F4/80⁻Ly6G⁺Ly6C^low^ neutrophils (*Ifna* and *Ifnb*: cisplatin/control ab n=2 animals, cisplatin/anti-CSF-1R n=4 animals) and CD45⁻CD11b⁻CD31⁻ tumor cells/fibroblasts (*Ifna*: n=4 animals/group; *Ifnb*: cisplatin/control ab n=4 animals, cisplatin/anti-CSF-1R n=3 animals) isolated from end-stage KEP tumors were determined by qPCR and normalized to β-actin. **(i)** Transcript of *Ifna* in cultured bone marrow-derived macrophages treated for 24h with either control antibody or anti-CSF-1R in the presence of KEP cancer cell line-derived conditioned medium. Data are representative of 4 independent experiments. Data presented in **a-c** and **f-h** are mean values ± SEM and statistical analysis was performed using two-tailed Mann–Whitney test. CIS, cisplatin; DOCE, docetaxel.
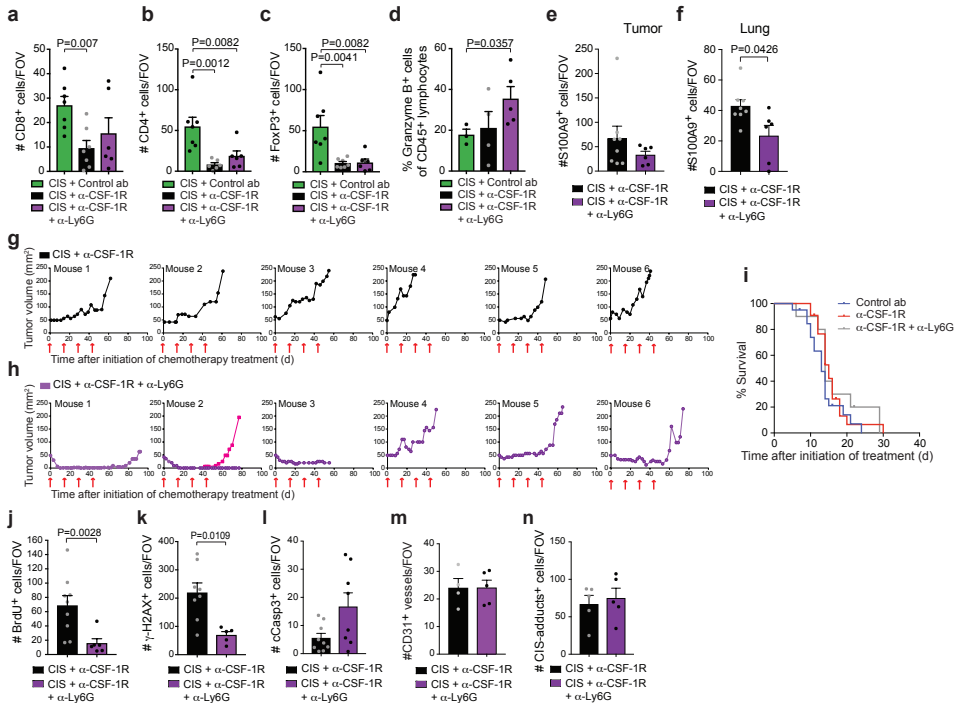
Supplementary Fig. 6 | Neutrophil inhibition enhances intratumoral granzyme B expression and improves the synergistic anti-cancer effect of cisplatin/anti-CSF-1R in *K14cre;Cdh1^{F/F};Trp53^{F/F}* mice. **(a-c)** Quantification of CD8$^+$ T cells **(a)**, CD4$^+$ T cells **(b)** and FoxP3$^+$ regulatory T cells **(c)** in viable areas of mammary tumors of time point-sacrificed KEP mice (CD8: cisplatin/control ab n=7 animals, cisplatin/anti-CSF-1R n=7 animals, cisplatin/anti-CSF-1R/anti-Ly6G n=7 animals; CD4: cisplatin/control ab n=7 animals, cisplatin/anti-CSF-1R n=6 animals, cisplatin/anti-CSF-1R/anti-Ly6G n=6 animals; FoxP3: cisplatin/control ab n=7 animals, cisplatin/anti-CSF-1R n=7 animals, cisplatin/anti-CSF-1R/anti-Ly6G n=6 animals). **(d)** Proportion of granzyme B$^+$ CD45$^+$ lymphocytes (lymphocyte gate was based on SSC and FSC) determined by flow cytometry in the tumor of time point-sacrificed KEP mice treated as indicated (cisplatin/control ab n=3 animals, cisplatin/anti-CSF-1R n=4 animals, cisplatin/anti-CSF-1R/anti-Ly6G n=5 animals). **(e-f)** Quantification of S100A9$^+$ cells in viable areas of mammary tumors **(e)** and lung **(f)** of end-stage KEP mice treated with cisplatin/anti-CSF-1R (n=8 animals) or cisplatin/anti-CSF-1R/anti-Ly6G (n=6 animals). **(g-h)** Representative tumor growth graphs of six individual KEP mice treated with cisplatin/anti-CSF-1R **(g)** and cisplatin/anti-CSF-1R/anti-Ly6G **(h)**. Data are representative of 16 cisplatin/anti-CSF-1R-treated mice and 10 cisplatin/anti-CSF-1R/anti-Ly6G-treated mice. Red arrows indicate cisplatin injections. In pink, growth curve of a secondary tumor that developed in another mammary gland during the treatment. **(i)** Kaplan-Meier tumor-specific survival curves of KEP mice treated with control ab, anti-CSF-1R (same groups as Fig. 1f) or anti-CSF-1R/anti-Ly6G (n=10 animals). **(j-n)** Quantification of BrdU$^+$ **(j)** γH2AX$^+$ cells **(k)**, cleaved caspase 3$^+$ cells **(l)**, CD31$^+$ vessels **(m)** and cisplatin adducts$^+$ cells **(n)** in viable areas of mammary tumors of time point-sacrificed KEP mice treated with cisplatin/anti-CSF-1R (same as Fig. 1h and Supplementary Fig. 2) and cisplatin/anti-CSF-1R/anti-Ly6G (BrdU n=6 animals; γH2AX n=5 animals; cCasp3 n=8 animals; CD31 n=5 animals; CIS adducts n=5 animals). Values presented in **a-c**, **e-f, j-l** and **n** represent average number of positive cells per field of view (FOV) as determined by IHC quantified by counting five high-power microscopic fields per tumor. Values presented in **m** represent average number of positive cells per FOV as determined by immunofluorescence by counting six field per tumor. Data presented in **a-f** and **j-n** are mean values ± SEM. Statistical analysis was performed using two-tailed Mann–Whitney test. CIS, cisplatin.

5

Supplementary Table 1: List of antibodies used

Immunohistochemistry

Antibody	Antigen retrieval	Clone	Vendor	Dilution	Catalog number
BrdU	TRIS/EDTA pH 9.0	Bu20a	DakoCytomation	1:100	M 0744
CD3	TRIS/EDTA pH 9.0	SP7	Thermo Scientific	1:600	RM-9107
CD4	TRIS/EDTA pH 9.0	4SM95	eBioscience	1:1000	14-9766-80
CD8	TRIS/EDTA pH 9.0	4SM15	eBioscience	1:2000	14-0808
FoxP3	Citrate buffer	FJK-16s	eBioscience	1:400	14-5773
F4/80	Proteinase K 20µg/ml	Cl:A3-1	AbD Serotec	1:400	MCA497
Granzyme B	Citrate buffer	-	Novus Biologicals	1:200	NB100-684
Ly6G	Proteinase K 20µg/ml	1A8	BD Biosciences	1:150	551459
Cleaved Caspase 3	TRIS/EDTA pH 9.0	-	Cell Signaling	1:400	#9661
CD34	TRIS/EDTA pH 9.0	MEC 14.7	Abcam	1:500	ab8158
γH2AX (Ser139)	Citrate buffer	-	Cell Signaling	1:50	#2577
S100A9	TRIS/EDTA pH 9.0	HPA004193	Atlas Antibodies	1:1000	HPA 004193
NKp46	PT module buffer 1 (Thermo, TA-250-PM1X)	-	R&D systems	1:100	AF2225
MBP	Pepsin solution	-	Lee Laboratory, Mayo Clinic	1:500	-
cytokeratin 8	Citrate buffer	Troma 1	Developmental Studies Hybridoma Bank, University of Iowa	1:600	Troma I

Cisplatin adducts	-	-	NKI-A59	1:100	-

Immunofluorescence

Antibody	Antigen retrieval	Clone	Vendor	Dilution	Catalog number
actin a-Smooth muscle-Cy3	Citrate Buffer	1A4	Sigma-Aldrich	1:200	C6198
CD31	Citrate Buffer	-	Abcam	1:200	ab28364
Donkey anti-rabbit AF647	-	-	Invitrogen, ThermoFisher Scientific,	1:500	A-31573

Flow cytometry

CSF-1R expression panel:

Antibody	Fluorophore	Clone	Vendor	Dilution	Catalog number
CD45	eVolve605	30-F11	eBioscience	1:100	83-0451-42
CD11b	BV650	M1/70	Biolegend	1:400	101239
F4/80	APCef780	BM8	eBioscience	1:200	47-4801-82
Ly6C	ef450	hk1.4	eBioscience	1:400	48-5932-82
Ly6G	AF700	1A8	Biolegend	1:200	127622
CD115 (CSF-1R)	PE	AFS98	eBioscience	1:200	12-1152-82
7AAD			eBioscience	1:20	00-6993-50

5

Intratumoral macrophage panel:

Antibody	Fluorophore	Clone	Vendor	Dilution	Catalog number
CD16/CD32	-	2.4G2	BD Biosciences	1:50	553141
CD45	BUV395	30-F11	BD Biosciences	1:200	564279
CD11b	BV650	M1/70	Biolegend	1:400	101239
F4/80	AF700	BM8	Biolegend	1:200	123130
MHCII	APCef780	M5/114.15.2	eBioscience	1:200	47-5321-82
CD206	AF488	MR5D3	AbD serotec	1:100	MCA2235
7AAD			eBioscience	1:20	00-6993-50

Tumor panel I:

Antibody	Fluorophore	Clone	Vendor	Dilution	Catalog number
CD45	eVolve605	30-F11	eBioscience	1:100	83-0451-42
CD11b	BV650	M1/70	Biolegend	1:400	101239
Ly6C	ef450	hk1.4	eBioscience	1:400	48-5932-82
Ly6G	AF700	1A8	Biolegend	1:200	127622
F4/80	FITC	BM8	eBioscience	1:200	11-4801-82
CD3	PE-cy7	145-2c11	eBioscience	1:200	17-0031-82
CD31	PercPef710	390	eBioscience	1:200	46-0311-82
Fixable Viability Dye eFluor® 780			eBioscience	1:1000	65-0865-14

Tumor panel II:

Antibody	Fluorophore	Clone	Vendor	Dilution	Catalog number
CD45	eVolve605	30-F11	eBioscience	1:100	83-0451-42
CD11b	BV650	M1/70	Biolegend	1:400	101239
F4/80	AF700	BM8	Biolegend	1:200	123130
CD103	PercPef710	2E7	eBioscience	1:200	46-1031-82
B220	FITC	RA3-6B2	eBioscience	1:200	11-0452-82
MHCII	APCef780	M5/114.15.2	eBioscience	1:200	47-5321-82
CD11c	PE-cy7	HL3	BD Biosciences	1:200	558079
CD3 (dump)	ef450	145-2c11	eBioscience	1:200	48-0031-82
CD19 (dump)	ef450	ebio1D3	eBioscience	1:200	48-0193-82
LIVE/ DEAD® Fixable Aqua Dead Cell Stain, for 405 nm excitation			ThermoFisher Scientific	1:100	L34957

5

tumor panel III (oxaliplatin-treated mice):

Antibody	Fluorophore	Clone	Vendor	Dilution	Catalog number
CD16/CD32	-	2.4G2	BD Biosciences	1:50	553141
CD45	APCef780	30-F11	eBioscience	1:200	47-0451-82
CD11b	BV786	M1/70	BD Biosciences	1:400	740861
Ly6C	BV605	hk1.4	Biolegend	1:400	128035
Ly6G	AF700	1A8	Biolegend	1:200	127622
F4/80	Ef450	BM8	eBioscience	1:200	48-4801-82
7AAD				1:20	00-6993-50

Lymphocyte panel:

Antibody	Fluorophore	Clone	Vendor	Dilution	Catalog number
CD45	eVolve605	30-F11	eBioscience	1:100	83-0451-42
CD3	PE-cy7	145-2c11	eBioscience	1:200	17-0031-82
CD8	PerCPef710	53-6.7	eBioscience	1:200	46-0081-82
CD4	PE-cy5	H129.19	BD Biosciences	1:200	553654
Granzyme B	PE	GB-11	Pelicluster Sanquin	1:100	M2289
F4/80 (dump)	APCef780	BM8	eBioscience	1:200	47-4801-82
CD11b (dump)	APCef780	M1/70	eBioscience	1:200	47-0112-82
CD19 (dump)	APCef780	ebio1D3	eBioscience	1:200	47-0193-82
Fixable Viability Dye eFluor® 780			eBioscience	1:1000	65-0865-14

Macrophage characterization panel 1:

Antibody	Fluorophore	Clone	Vendor	Dilution	Catalog number
CD16/ CD32	-	2.4G2	BD Biosciences	1:50	553141
CD45	BUV395	30-F11	BD Biosciences	1:200	564279
CD11b	BV650	M1/70	Biolegend	1:400	101239
F4/80	FITC	BM8	eBioscience	1:200	11-4801-82
Ly6C	PE/Dazzle	hk1.4	Biolegend	1:400	128044
MHCII	APCef780	M5/114.15.2	eBioscience	1:200	47-5321-82
CD11c	PE-cy7	HL3	BD Biosciences	1:200	558079
CD80	PerCPef710	16-10A1	eBioscience	1:200	46-0801-82
CD86	PE	GL1	eBioscience	1:400	12-0862-82
Siglec F	BV605	E50-2440	BD Biosciences	1:200	740388
Ly6G	AF700	1A8	Biolegend	1:200	127622
CD3 (dump)	ef450	145-2c11	eBioscience	1:200	48-0031-82
CD19 (dump)	ef450	ebio1D3	eBioscience	1:200	48-0193-82
CD49b (dump)	ef450	DX5	eBioscience	1:200	48-5971-82
DAPI			Sigma-Aldrich	1:20	D9542

5

Macrophage characterization panel 2:

Antibody	Fluorophore	Clone	Vendor	Dilution	Catalog number
CD16/ CD32	-	2.4G2	BD Biosciences	1:50	553141
CD45	BUV395	30-F11	BD Biosciences	1:200	564279
CD11b	BV650	M1/70	Biolegend	1:400	101239
F4/80	AF700	BM8	Biolegend	1:200	123130
Ly6C	PE/Dazzle	hk1.4	Biolegend	1:400	128044
MHCII	APCef780	M5/114.15.2	eBioscience	1:200	47-5321-82
CD274	PerCPef710	MIH5	eBioscience	1:200	46-5982-82
Siglec F	BV605	E50-2440	BD Biosciences	1:200	740388
Ly6G (dump)	ef450	1A8	eBioscience	1:400	48-9668-82
CD3 (dump)	ef450	145-2c11	eBioscience	1:200	48-0031-82
CD19 (dump)	ef450	ebio1D3	eBioscience	1:200	48-0193-82
CD49b (dump)	ef450	DX5	eBioscience	1:200	48-5971-82
DAPI			Sigma-Aldrich	1:20	D9542

Macrophage characterization panel 3:

Antibody	Fluorophore	Clone	Vendor	Dilution	Catalog number
CD16/ CD32	-	2.4G2	BD Biosciences	1:50	553141
CD45	BUV395	30-F11	BD Biosciences	1:200	564279
CD11b	BV650	M1/70	Biolegend	1:400	101239
F4/80	FITC	BM8	eBioscience	1:200	11-4801-82
Ly6C	PE/Dazzle	hk1.4	Biolegend	1:400	128044
MHCII	APCef780	M5/114.15.2	eBioscience	1:200	47-5321-82
CCR2	PE	475301	R&D systems	1:100	FAB5538P-025
CX3CR1	APC	SA011F11	Biolegend	1:400	149008
Siglec F	BV605	E50-2440	BD Biosciences	1:200	740388
Ly6G (dump)	ef450	1A8	eBioscience	1:400	48-9668-82
CD3 (dump)	ef450	145-2c11	eBioscience	1:200	48-0031-82
CD19 (dump)	ef450	ebio1D3	eBioscience	1:200	48-0193-82
CD49b (dump)	ef450	DX5	eBioscience	1:200	48-5971-82
DAPI			Sigma-Aldrich	1:20	D9542

5

Macrophage characterization in K14cre;Trp53$^{F/F}$ tumor panel 1:

Antibody	Fluorophore	Clone	Vendor	Dilution	Catalog number
CD16/CD32	-	2.4G2	BD Biosciences	1:50	553141
CD45	BUV395	30-F11	BD Biosciences	1:200	564279
CD11b	BV786	M1/70	BD Biosciences	1:400	740861
F4/80	APCef780	BM8	eBioscience	1:200	47-4801-82
Ly6C	ef450	hk1.4	eBioscience	1:400	48-5932-82
Ly6G	FITC	1A8	BD Biosciences	1:200	551460
Siglec F	BV605	E50-2440	BD Biosciences	1:200	740388
CD86	PE	GL1	eBioscience	1:400	12-0862-82
CX3CR1	APC	SA011F11	Biolegend	1:400	149008
CD80	PercPef710	16-10A1	eBioscience	1:200	46-0801-82
CD274	PEcy7	MIH5	eBioscience	1:200	25-5982-82
7AAD				1:20	00-6993-50

Macrophage characterization in K14cre;Trp53$^{F/F}$ tumor panel 2:

Antibody	Fluorophore	Clone	Vendor	Dilution	Catalog number
CD16/CD32	-	2.4G2	BD Biosciences	1:50	553141
CD45	BUV395	30-F11	BD Biosciences	1:200	564279
CD11b	BV786	M1/70	BD Biosciences	1:400	740861
F4/80	APCef780	BM8	eBioscience	1:200	47-4801-82
Ly6C	ef450	hk1.4	eBioscience	1:400	48-5932-82
Ly6G	AF700	1A8	Biolegend	1:200	127622
Siglec F	BV605	E50-2440	BD Biosciences	1:200	740388
CCR2	PE	475301	R&D systems	1:200	FAB5538P-025
7AAD				1:20	00-6993-50

tdTomato⁺ monocyte panel:

Antibody	Fluorophore	Clone	Vendor	Dilution	Catalog number
CD16/ CD32	-	2.4G2	BD Biosciences	1:50	553141
CD45	BUV395	30-F11	BD Biosciences	1:200	564279
CD11b	BV786	M1/70	BD Biosciences	1:400	740861
F4/80	APCef780	BM8	eBioscience	1:200	47-4801-82
Ly6C	ef450	hk1.4	eBioscience	1:400	48-5932-82
Ly6G	AF700	1A8	Biolegend	1:200	127622
Siglec F	BV605	E50-2440	BD Biosciences	1:200	740388
CCR2	AF488	475301	R&D systems	1:200	FAB55381RG-100UG
CX3CR1	APC	SA011F11	Biolegend	1:400	149008
CD80	PercPef710	16-10A1	eBioscience	1:200	46-0801-82
CD274	PEcy7	MIH5	eBioscience	1:200	25-5982-82
7AAD				1:20	00-6993-50

5

Isolation of mTmG monocytes from bone marrow:

Antibody	Fluorophore	Clone	Vendor	Dilution	Catalog number
CD11b	BV786	M1/70	BD Biosciences	1:400	740861
Ly6C	Ef450	hk1.4	eBioscience	1:400	48-5932-82
Siglec F	BV605	E50-2440	BD Biosciences	1:200	740388
cKIT	BV605	2B8	BD Biosciences	1:200	563146
Sca1	BV605	D7	Biolegend	1:200	108133
CD3	FITC	145-2C11	eBioscience	1:200	11-0031-63
CD8	FITC	53-6.7	eBioscience	1:400	11-0081-82
CD4	FITC	GK1.5	eBioscience	1:400	11-0041-82
NKp46	FITC	29A1.4	eBioscience	1:200	11-3351-82
Ter119	FITC	TER-119	Biolegend	1:200	116205
F4/80	APCef780	BM8	eBioscience	1:200	47-4801-82
7AAD			eBioscience	1:20	00-6993-50

Isolation of cells populations from intratumoral CD11b$^+$ fraction:

Antibody	Fluorophore	Clone	Vendor	Dilution	Catalog number
Ly6G	FITC	1A8	BD Biosciences	1:200	551460
F4/80	PE	BM8	eBioscience	1:200	12-4801-82
Ly6C	Ef450	hk1.4	eBioscience	1:400	48-5932-82

Isolation of cells populations from intratumoral CD11b⁻ fraction:

Antibody	Fluorophore	Clone	Vendor	Dilution	Catalog number
CD45	PercPcy5.5	30-F-11	eBioscience	1:200	45-0451-82
B220	PE-Cy7	RA3-6B2	eBioscience	1:200	25-0452-82
CD31	FITC	390	eBioscience	1:200	11-0311-82
CD11c	PE	N418	eBioscience	1:200	12-0114-82
MHCII	APCef780	M5/114.15.2	eBioscience	1:200	47-5321-82
CD19	Ef450	eBio1D3	eBioscience	1:200	48-0193-82
LIVE/ DEAD® Fixable Aqua Dead Cell Stain, for 405 nm excitation			ThermoFisher Scientific	1:100	L34957

5

Supplementary Table 2: List of primer sequences used for RT-PCR.

Gene	Primer Forward (5'-3')	Primer Reverse (5'-3')
IFNα (all genes)	TCTGATGCAGCAGGTGGG	AGGGCTCTCCAGACTTCTGCTCTG
IFNβ	GCACTGGGTGGAATGAGACT	AGTGGAGAGCAGTTGAGGACA
TLR3	GTGAGATACAACGTAGCTGACTG	TCCTGCATCCAAGATAGCAAGT
RIG-1	CCACCTACATCCTCAGCTACATGA	TGGGCCCTTGTTGTTCTTCT
IFIH1	GTGATGACGAGGCCAGCAGTTG	ATTCATCCGTTTCGTCCAGTTTCA
ISG15	GGTGTCCGTGACTAACTCCAT	TGGAAAGGGTAAGACCGTCCT
OAS1A	GCCTGATCCCAGAATCTATGC	GAGCAACTCTAGGGCGTACTG
β-actin	CCTCATGAAGATCCTGACCGA	TTTGATGTCACGCACGATTTC

Supplementary Table 3: List of type I IFN-related pathways and genes

List of type I IFN-related pathways and corresponding genes selected from BiNGO and Ingenuity Pathway Analysis (IPA) that are differentially expressed in neutrophils from cisplatin/anti-CSF-1R-treated tumors (n=4 biological independent samples) compared to neutrophils from cisplatin/control ab-treated tumors (n=3 biological independent samples). Statistical analysis was performed using two-way ANOVA

Biological processes by BiNGO Analysis	Genes	Fold change	p-value
POSITIVE REGULATION OF RESPONSE TO CYTOKINE STIMULUS	ZBP1	3.91	0.0027
	IRF7	3.17	0.0014
	NLRC5	2.84	0.0065
REGULATION OF RESPONSE TO CYTOKINE STIMULUS	ZBP1	3.91	0.0027
	IRF7	3.17	0.0014
	NLRC5	2.84	0.0065
REGULATION OF CYTOKINE-MEDIATED SIGNALING PATHWAY	ZBP1	3.91	0.0027
	IRF7	3.17	0.0014
	NLRC5	2.84	0.0065
REGULATION OF INNATE IMMUNE RESPONSE	ZBP1	3.91	0.0027
	IRF7	3.17	0.0014
	NLRC5	2.84	0.0065
	TAP1	2.8	0.0052
	DHX58	3.32	0.0006
REGULATION OF TYPE I INTERFERON-MEDIATED SIGNALING PATHWAY	ZBP1	3.91	0.0027
	IRF7	3.17	0.0014
	NLRC5	2.84	0.0065

5

POSITIVE REGULATION OF TYPE I INTERFERON-MEDIATED SIGNALING PATHWAY	ZBP1	3.91	0.0027
	IRF7	3.17	0.0014
	NLRC5	2.84	0.0065
POSITIVE REGULATION OF CYTOKINE-MEDIATED SIGNALING PATHWAY	ZBP1	3.91	0.0027
	IRF7	3.17	0.0014
	NLRC5	2.84	0.0065
NEGATIVE REGULATION OF TYPE I INTERFERON PRODUCTION	GBP4	11	0.002
	DHX58	3.32	0.0006
REGULATION OF TYPE I INTERFERON PRODUCTION	IRF7	3.17	0.0014
	GBP4	11	0.002
	DHX58	3.32	0.0006
REGULATION OF INTERFERON-ALPHA PRODUCTION	IRF7	3.17	0.0014
	GBP4	11	0.002
CELLULAR RESPONSE TO INTERFERON-BETA	IFI205	4.68	0.0073
	GBP2B	3.79	8.40E-05
	TREX1	2.86	6.10E-05
	GBP2	2.78	0.0043
	IFI202B	2.94	0.011
	IFIT1	2.89	0.0002
	IFIT3	3.58	0.0001

Biological processes by IPA	Genes	Fold change	p-value
RESPONSE TO INTERFERON-BETA	IFI205	4.68	0.0073
	GBP2B	3.79	8.40E-05
	TREX1	2.86	6.10E-05
	GBP2	2.78	0.0043
	XAF1	3.89	0.0029
	IFI202B	2.94	0.011
	IFIT1	2.89	0.0002
	IFIT3	3.58	0.0001
RESPONSE TO INTERFERON-ALPHA	IFIT1	2.89	0.0002
	IFIT3	3.58	0.0001
	IFIT2	3.42	0.0003
CELLULAR RESPONSE TO INTERFERON-ALPHA	IFIT1	2.89	0.0002
	IFIT3	3.58	0.0001
	IFIT2	3.42	0.0003
DEFENSE RESPONSE TO VIRUS	ZBP1	3.91	0.0027
	GBP2B	3.79	8.40E-05
	RSAD2	3.14	0.0063
	MX2	3.02	0.001
	IFIT1	2.89	0.0002
	IFIT3	3.58	0.0001
	IFIT2	3.42	0.0003
	CXCL10	2.75	0.0005
	DHX58	3.32	0.0006

5

	IFI35	2.02	0.0066
	IFIT1	2.89	0.0002
	IFIT3	3.58	0.0001
	IFITM3	2.42	0.002
	IRF1	2.25	0.0006
	IRF9	2.12	0.0015
INTERFERON SIGNALING	MX2	3.02	0.001
	OAS1a	2.37	0.0023
	OAS1g	4.21	0.0008
	PSMB8	1.97	0.0465
	SOCS1	2.59	0.0176
	STAT1	2.24	0.0029
	STAT2	2.46	0.0002
	TAP1	2.8	0.0052
	ADAR	1.67	0.0463
	DHX58	3.32	0.0006
	IFIH1	2.38	0.0009
	IFIT2	3.42	0.0003
ACTIVATION OF IRF BY CYTOSOLIC PATTERN RECOGNITION RECEPTORS	IRF7	3.17	0.0014
	IRF9	2.12	0.0015
	ISG15	2.46	0.0022
	STAT1	2.24	0.0029
	STAT2	2.46	0.0002
	ZBP1	3.91	0.0027

5